nature chemical biology

Article

https://doi.org/10.1038/s41589-023-01412-4

β-Arrestin-independent endosomal cAMP signaling by a polypeptide hormone GPCR

Received: 2 September 2022

Accepted: 26 July 2023

Published online: 25 September 2023

Check for updates

Emily E. Blythe [1] & Mark von Zastrow [1,2,3]

Many G protein-coupled receptors (GPCRs) initiate a second phase of stimulatory heterotrimeric G protein (G_s)-coupled cAMP signaling after endocytosis. The prevailing current view is that the endosomal signal is inherently β-arrestin-dependent because β-arrestin is necessary for receptor internalization and, for some GPCRs, to prolong the endosomal signal. Here we revise this view by showing that the vasoactive intestinal peptide receptor 1 (VIPR1), a secretin-family polypeptide hormone receptor, does not require β-arrestin to internalize or to generate an endosomal signal. β-Arrestin instead resolves the plasma membrane and endosomal signaling phases into sequential cAMP peaks by desensitizing the plasma membrane phase without affecting the endosomal phase. This appears to occur through the formation of functionally distinct VIPR1–β-arrestin complexes at each location that differ in their phosphorylation dependence. We conclude that endosomal GPCR signaling can occur in the absence of β-arrestin and that β-arrestin sculpts the spatiotemporal profile of cellular GPCR–G protein signaling through location-specific remodeling of GPCR–β-arrestin complexes.

GPCRs comprise the largest class of signaling receptors, regulate essentially every physiological process and are important drug targets[1]. Upon binding agonist ligands, GPCRs engage cognate heterotrimeric G proteins to transduce signaling through specific downstream effectors[2,3]. The biochemical basis of GPCR–G protein activation has been studied to a level of atomic detail[4,5], but we are only now beginning to understand the subcellular organization of GPCR signaling[2,6,7]. Many GPCRs are not restricted to the plasma membrane and transit the endocytic pathway[8]. However, endocytosis was long believed only to impact the longer-term homeostatic regulation of GPCRs and not affect the response to acute agonist application. This view has changed due to the accumulation of substantial evidence that various GPCRs have the capacity to engage G proteins after endocytosis, as well as from the plasma membrane, and can leverage the endocytic network to promote or sustain cellular signaling[2,6,7].

Support for this still-evolving view is well-developed for GPCRs that signal by coupling to stimulatory heterotrimeric G proteins (G_s) which activate adenylyl cyclases to produce cAMP. A number of such GPCRs have now been shown to engage G_s on the endosome limiting membrane as well as the plasma membrane, enabling receptors to initiate sequential 'waves' of signaling from each location[2,6,9–15]. Numerous studies have demonstrated striking differences in the downstream effects of cAMP generated at the plasma membrane compared with internal membrane compartments, both at the cell and tissue levels[9,11,13–19], highlighting how spatiotemporal aspects of GPCR activation can profoundly influence functional responses through cAMP. Yet, how such signaling diversity is programmed remains poorly understood.

GPCR-elicited cellular cAMP signaling can be determined by many factors, including the ligand's binding affinity for receptors[10,11] and specific features of the receptor's trafficking itinerary[20,21]. One important factor is the interaction between GPCRs and β-arrestin. β-Arrestins (β-arrestin-1 (β-arr1) and β-arrestin-2 (β-arr2); also called Arrestin 2 and Arrestin 3) were discovered as scaffolding proteins which are recruited to and functionally desensitize activated receptors at the plasma membrane[22]. β-Arrestins additionally function as essential endocytic adaptor proteins for many GPCRs, promoting receptor

[1]Department of Psychiatry and Behavioral Sciences, University of California, San Francisco, San Francisco, CA, USA. [2]Department of Cellular and Molecular Pharmacology, University of California, San Francisco, San Francisco, CA, USA. [3]Quantitative Biology Institute, University of California, San Francisco, San Francisco, CA, USA. e-mail: mark.vonzastrow@ucsf.edu

endocytosis via clathrin-coated pits and driving receptor delivery to endosomes[22,23]. Polypeptide hormone receptors provide particularly clear examples of such behavior. In particular, the thyroid stimulating hormone receptor (TSHR), parathyroid hormone receptor-1 (PTHR1) and vasopressin-2 receptor (V2R) have all been extensively shown to produce a cAMP signal from the endosome membrane that is inherently β-arrestin-dependent because β-arrestin is required for receptors to internalize[9–11,17,18,24–27]. In addition, for the PTHR1 and V2R, persistent binding to β-arrestin after internalization has been shown to sustain the endosomal cAMP signal[2,11,24–29]. Accordingly, a prevailing current view in the field is that GPCR signaling from endosomes is strictly β-arrestin-dependent. There has been evidence for many years that some GPCRs can internalize independently of β-arrestin[23,30], and some of these have been shown to produce an endosomal cAMP signal (for example, see ref. 14). However, to our knowledge, it is not known if any GPCR can produce endosomal G_s activation in the absence of cellular β-arrestin. If so, a fundamental next question that arises is whether or how β-arrestin affects the GPCR-elicited cellular cAMP response.

Here, we address these questions by focusing on the vasoactive intestinal peptide receptor 1 (VIPR1 or VPAC1) as a model secretin-subfamily polypeptide hormone GPCR shown previously to associate with β-arrestin at both the plasma membrane and endosome, but whose internalization is insensitive to a dominant negative mutant of β-arrestin[30,31]. We show that agonist-induced VIPR1 endocytosis is indeed β-arrestin-independent and then leverage this property to disentangle effects of β-arrestin binding and endocytosis on the cellular cAMP signal produced by endogenous receptor activation. While β-arrestin is clearly not required for endosomal G_s activation or cAMP signaling by VIPR1, we show that it plays a different role in temporally resolving the effects of VIPR1-G_s activation from the plasma membrane and endosomes into separate and sequential peaks of global cytoplasmic cAMP elevation. The present results provide, to our knowledge, the first direct example of a GPCR for which G_s-cAMP signaling from endosomes has been explicitly shown to be fully β-arrestin-independent and reveal a discrete function of β-arrestin in spatiotemporally sculpting the cell's overall cAMP response through the formation of distinct GPCR–β-arrestin complexes at the plasma membrane and endosomes.

Results

VIPR1 is internalized in β-arrestin double knockout cells

To determine whether VIPR1 could serve as a model receptor to disentangle the effects of β-arrestin on trafficking and signaling, we first set out to characterize VIPR1 internalization in HEK293 cells. To do so, we used a cell-impermeant HaloTag dye (JF_{635}i-HTL) to selectively label receptors in the plasma membrane of living cells[32]. As expected[30,31,33,34], HaloTag-VIPR1 underwent endocytosis in wild-type cells upon addition of its agonist, vasoactive intestinal peptide (VIP) (Fig. 1a). Surface-labeled receptors were visible in intracellular puncta that colocalized with both an overexpressed DsRed-labeled EEA1 and endogenous EEA1 (Extended Data Fig. 1a–c), identifying these structures as early endosomes. Some receptor-positive endosomes were visible even before VIP application, suggesting a low level of constitutive (agonist-independent) endocytosis. However, VIP markedly increased receptor localization in DsRed2-EEA1-positive endosomes, confirming that VIPR1 endocytosis is stimulated by agonist (Extended Data Fig. 1a). Agonist-induced internalization was further verified and quantified using flow cytometry, which showed an extremely rapid loss of surface receptor labeling that reached completion within 10 min of treatment with VIP (Fig. 1b). Both constitutive and agonist-induced components of VIPR1 internalization were observed under conditions in which VIPR1 expression level varies, though higher VIPR1 expression led to lower apparent levels of internalization (Extended Data Fig. 1d,e)[34].

After establishing that VIPR1 undergoes agonist-induced internalization, we next explored its basic mechanistic properties. Similar to many other GPCRs, and consistent with previous studies[30,31], VIPR1 endocytosis was dynamin-dependent, as overexpression of a dominant negative mutant of dynamin 1 (Dyn1-K44E) fully suppressed agonist-induced internalization (Fig. 1c). Previous evidence relevant to β-arrestin-dependence was based on insensitivity of VIPR1 to endocytic inhibition by dominant negative mutant constructs overexpressed on a wild-type background[30,31]. To test the requirement for β-arrestin in VIPR1 internalization more incisively, we examined the effect of depleting endogenous β-arrestin. We generated two independent mutant HEK293 cell lines lacking both β-arr1 and β-arr2 using CRISPR. We validated complete β-arrestin knockout (KO) in both β-arrestin double knockout (β-arr DKO) cell lines biochemically, by genomic DNA sequencing and western blotting (Extended Data Fig. 2a,b), and functionally by loss of β2-adrenergic receptor (β2AR) internalization (a β-arrestin-dependent GPCR) (Fig. 1d). Robust internalization of VIPR1 was still observed in β-arr DKO cells, and complete depletion of β-arrestin did not affect the degree or kinetics of agonist-induced internalization in either independent cell line (Fig. 1d and Extended Data Fig. 2c). Therefore, agonist-induced endocytosis of VIPR1 proceeds through a dynamin-dependent, β-arrestin-independent mechanism.

VIPR1 mediates membrane recruitment of β-arrestin

As VIPR1 internalization does not require β-arrestin, we wanted to confirm that VIPR1 indeed recruits β-arrestin after activation, as previously reported[31]. Live confocal fluorescence imaging demonstrated visible membrane recruitment of β-arr1 after VIP application, first to the plasma membrane and then to endosomes containing internalized VIPR1 (Fig. 1e). We further quantified this sequential β-arrestin recruitment phenotype with a nanoluciferase protein complementation (NanoBiT) assay using CAAX motif or endofin-derived FYVE domain constructs as previously validated markers of the plasma membrane and endosome membrane, respectively (Extended Data Fig. 3)[35]. Using this 'bystander' assay, we observed sequential recruitment of β-arr2 after VIP-induced activation of VIPR1, first to the plasma membrane and then to the endosome membrane, with the transition between the two being nearly complete within 5 min (Fig. 1f).

VIPR1 signals at the plasma membrane and endosomes

These above results indicate that VIPR1 robustly recruits β-arrestin and remains bound to β-arrestin in endosomes, yet it does not require β-arrestin for endocytosis. To our knowledge, these characteristics differentiate VIPR1 from all other GPCRs for which the β-arrestin-dependence of endosomal signaling has been explicitly investigated. This motivated us to ask if VIPR1 is able to generate an endocytosis-dependent cAMP signaling phase.

VIPR1 is natively expressed in the kidney[36], and previous studies have documented endogenous VIPR1 expression in HEK293 cells[31,37,38]. We first sought to independently verify that endogenous VIPR1 is indeed responsible for the VIP-elicited cAMP elevation measured in our cell model. CRISPR-mediated KO of VIPR1 strongly suppressed the cytoplasmic cAMP elevation elicited by VIP application, as measured in living cells using a genetically encoded fluorescent cAMP biosensor (cADDis), while VIPR2 KO had little effect (Extended Data Fig. 4a,b). A small residual cAMP response was still present in VIPR1 KO cells, and other secretin-family GPCRs—notably the secretin and pituitary adenylate cyclase-activating polypeptide (PACAP) receptors—are also sensitive to VIP[39,40]. The PACAP 1 receptor (PAC1R) agonist PACAP-27 produced a detectable cAMP response exceeding that produced by VIP in VIPR1 KO cells, while secretin had no detectable effect (Extended Data Fig. 4c). These observations suggest that the residual VIP response is mediated by low-level expression of PAC1R, which displays a ~100-fold lower half-maximum effective concentration (EC_{50}) for PACAP-27 versus VIP (Extended Data Fig. 4d)[40] and has been detected in HEK293 by RNA sequencing[38]. However, as this residual contribution to the cellular

https://doi.org/10.1038/s41589-023-01412-4

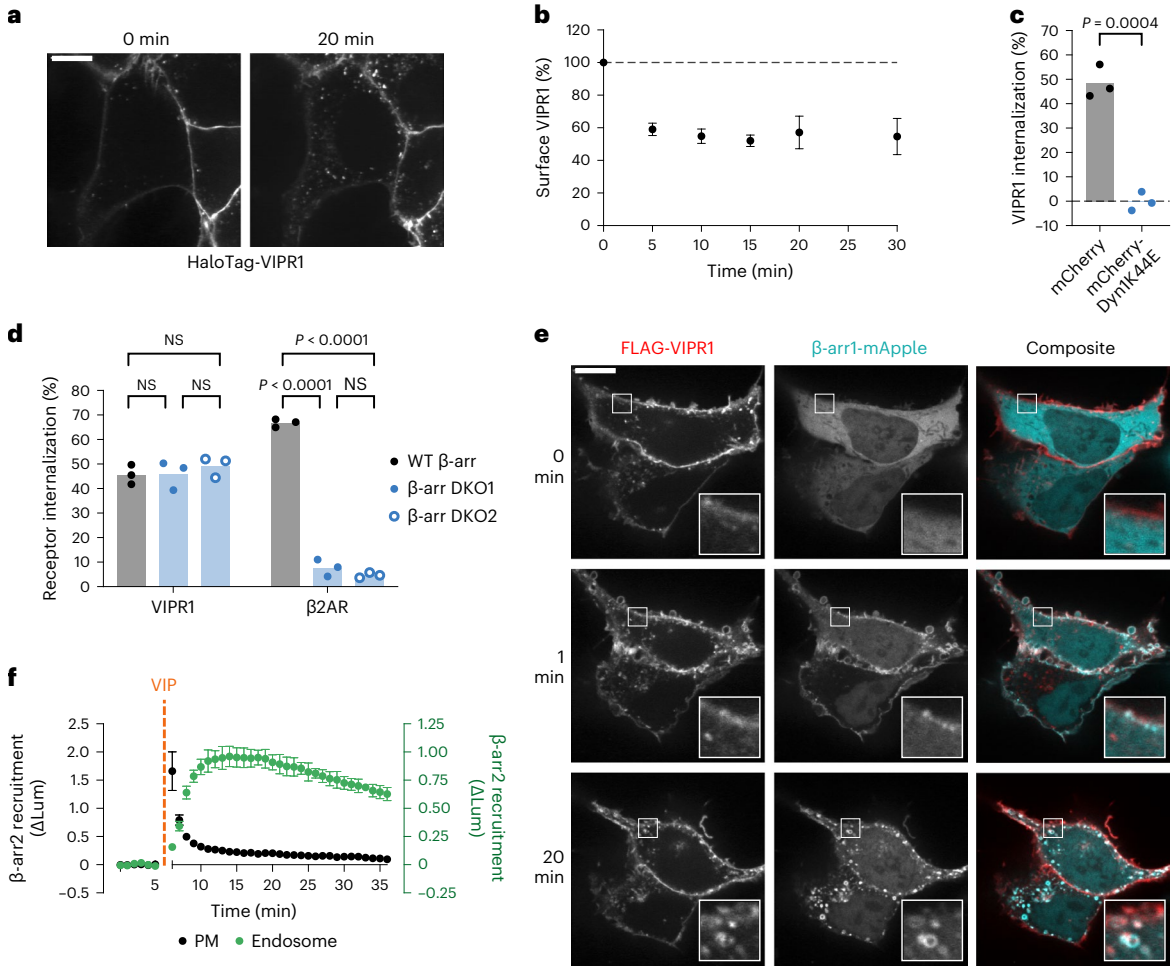

Fig. 1 | β-Arrestin is recruited to activated VIPR1 but is not required for its internalization. a, Representative stills ($n = 3$) from time-lapse microscopy of cells expressing HaloTag-VIPR1 immediately before or 20 min after stimulation with 500 nM VIP. HaloTag-VIPR1 was expressed under a doxycycline (Dox)-inducible promoter, and surface receptor was labeled with cell-impermeant JF_{635}i-HTL for 10 min before imaging. Scale bar, 10 µm. **b**, Time course of surface levels of HaloTag-VIPR1 after 500 nM VIP treatment, as measured by flow cytometry. **c**, Internalization of HaloTag-VIPR1 in cells co-expressing mCherry-Dyn1K44E or mCherry after a 30-min treatment with 500 nM VIP, as measured by flow cytometry. Significance was determined by an unpaired two-sided *t*-test. **d**, Internalization of HaloTag-VIPR1 and HaloTag-β2AR after a 30-min treatment with 500 nM VIP or a 20-min treatment with 1 µM isoproterenol, respectively, in cell lines expressing endogenous β-arrestin (WT β-arr) or lacking β-arrestin (β-arr DKO1 and β-arr DKO2). Receptor internalization was measured by flow cytometry, and significance was determined by a two-way analysis of variance (ANOVA) with Tukey's multiple comparisons test. **e**, Representative stills ($n = 5$) from time-lapse microscopy of WT HEK293 cells co-expressing FLAG-VIPR1 and β-arr1-mApple, with 500 nM VIP added at 0 min. Surface FLAG-VIPR1 was labeled with anti-FLAG M1 antibody conjugated to Alexa Fluor 647 for 10 min before imaging. Scale bar, 10 µm. **f**, NanoBiT bystander assays showing recruitment of β-arr2-smBiT to the plasma membrane (LgBiT-CAAX, black) or the endosome (endofin-LgBiT, green), as measured by a change in luminescence (ΔLum) upon addition of 1 µM VIP at 5 min. All data represent three biological replicates, shown as individual data points or mean ± s.d. NS, not significant; PM, plasma membrane; WT, wild-type.

cAMP elevation is very small when compared with the VIPR1-mediated response (Extended Data Fig. 4b), we conclude that VIPR1 is indeed the major endogenous GPCR mediating the VIP-induced cAMP elevation measured in this study.

Next, we characterized the time course of the VIP-induced cAMP signal, as defined for these experiments by elevation of global cAMP concentration in living cells at 37 °C. Stimulation of HEK293 cells with VIP elicited a complex signal, characterized by an initial phase of cAMP elevation that peaked within <1 min and desensitized over ~5 min followed by a second, less intense peak and a later plateau of cAMP elevation that persisted above baseline in the prolonged presence of VIP (Fig. 2a, black curve). Both signaling phases were lost in VIPR1 KO cells, indicating that both are mediated by VIPR1 (Extended Data Fig. 4a). Furthermore, analysis of cAMP dynamics using quantitative fluorescence microscopy detected both phases in individual cells (Extended Data Fig. 4e). Accordingly, both phases of the complex VIP-induced cellular cAMP signal occur in the same cells and are mediated by endogenous VIPR1.

To investigate how endocytic trafficking impacts this overall cellular cAMP signal, we examined the effect of experimentally imposing endocytic blockade on the global cytoplasmic cAMP elevation. Preventing dynamin-dependent endocytosis of VIPR1 using a chemical inhibitor, Dyngo4a, abolished the second cAMP peak and subsequent plateau elevation without detectably affecting the first peak (Fig. 2a, blue curve, and Supplementary Table 1). Genetically imposing endocytic inhibition with Dyn1-K44E also selectively blocked the second phase (Extended Data Fig. 4f). These results are consistent with the VIPR1-mediated cellular cAMP elevation being composed of two sequential phases: a first phase from the plasma membrane producing an initial peak of global cAMP elevation, and then a second phase from endosomes producing a subsequent peak and plateau. We further noted that cells pretreated with VIP exhibited an elevated baseline

https://doi.org/10.1038/s41589-023-01412-4

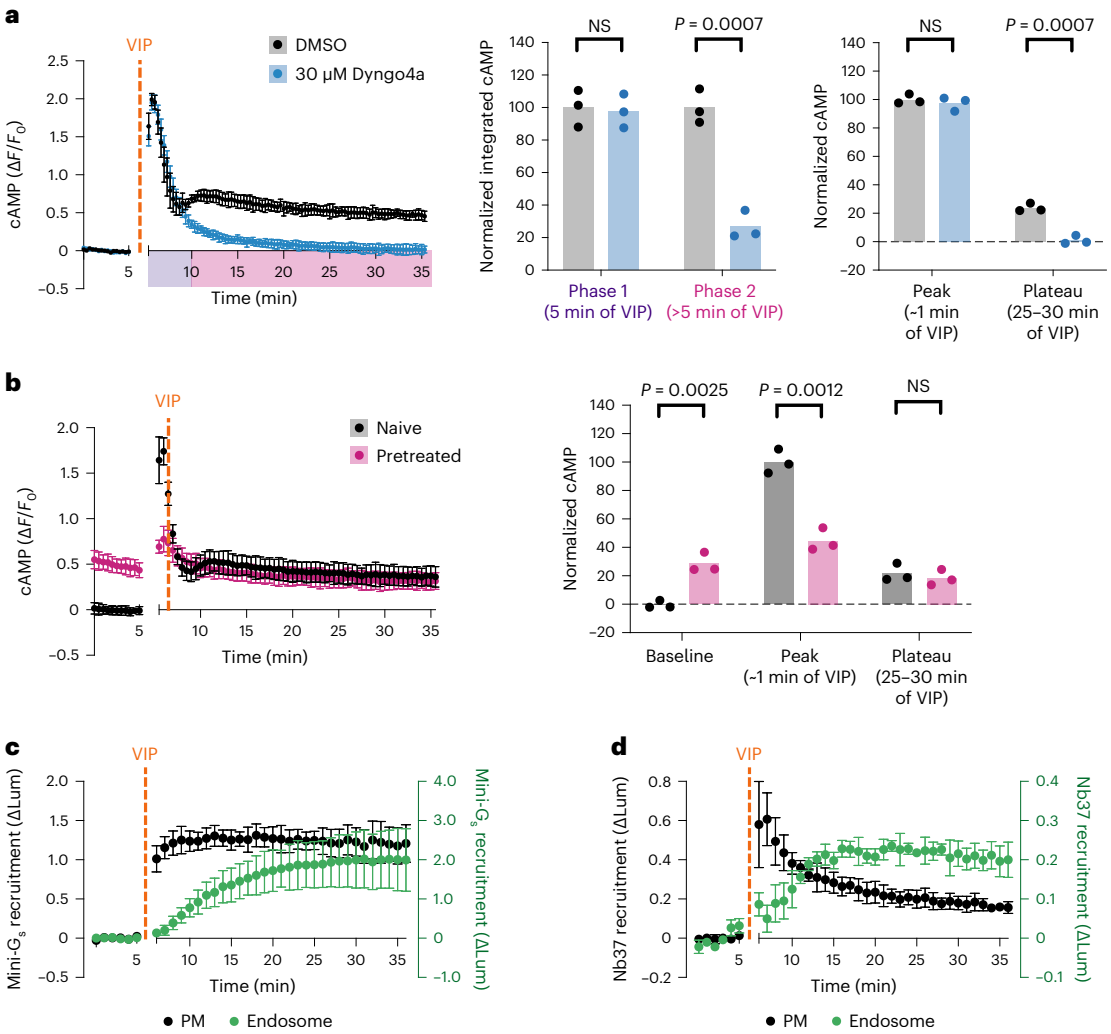

Fig. 2 | cAMP signaling through endogenous VIPR1 is biphasic. a, Intracellular cAMP, as measured by the fluorescence change of cADDis cAMP biosensor, upon treatment with 500 nM VIP added at 5 min. Cells were pretreated with 30 μM Dyngo4a (blue, $n = 4$) or DMSO (black, $n = 3$) for 10 min. Integrated cAMP of two phases (0–5 min and 5–30 min of VIP treatment) was calculated as the area under the curve and normalized to the average DMSO value. Normalized changes in fluorescence for the peak (maximum $\Delta F/F_0$) and the plateau (average for timepoints at 25–30 min of VIP treatment) were normalized to the average DMSO peak value. Significance was determined by unpaired two-sided *t*-tests. **b**, Changes in cAMP in cells pretreated with VIP ('Pretreated', pink) compared with those not ('Naive', black). Pretreated samples were treated with 500 nM VIP for 10 min, followed by a 10-min washout period before the acquisition of baseline measurements. Baseline (average for 5 min baseline), peak and plateau $\Delta F/F_0$ values were quantified as in **a**, with data normalized to the average naive peak value. Significance was determined by unpaired two-sided *t*-tests. $n = 3$. **c**,**d**, NanoBiT bystander assays showing recruitment of mini-G_s (**c**, $n = 5$) or Nb37 (**d**, $n = 3$) to the plasma membrane (black) or the endosome (green) upon addition of 1 μM VIP at 5 min. For all panels, data represent biological replicates and are shown as individual data points or mean ± s.d.

cAMP that persisted after VIP washout, whereas rechallenge with VIP was unable to produce a subsequent additional elevation (Fig. 2b). These results suggest that endosomal cAMP signaling by VIPR1 can be sustained even after agonist removal, despite the plasma membrane signal being terminated and desensitized within several minutes.

To further validate the subcellular location(s) of ligand-dependent VIPR1 and G_s activation, we took advantage of conformational biosensors that detect either active-state VIPR1 (mini-G_s) (refs. 41,42) or a conformational intermediate in the process of G_s activation (Nb37) (refs. 12,43). Using these tools in NanoBiT bystander assays, we observed that VIP promoted the recruitment of both biosensors first to the plasma membrane and then to endosomes (Fig. 2c,d). These results suggest that VIP-induced activation of VIPR1 and G_s occurs at both membrane locations, sequentially and with kinetics consistent with the biphasic cytoplasmic cAMP elevation measured using the cAMP biosensor.

VIPR1 signaling from endosomes is β-arrestin-independent

Having established the unique spatial and temporal profile of VIPR1-mediated cAMP signaling, we next asked how β-arrestin regulates it given that VIPR1 trafficking is β-arrestin-independent. To investigate this, we first compared endogenous VIPR1-mediated cAMP signaling produced in β-arr DKO cells with that produced in the parental (wild-type) cell background. In β-arr DKO cells, VIP elicited a rapid cAMP peak followed by a decay (Fig. 3a and Extended Data Fig. 5a). Calculating first derivatives and fitting decay time constants to these curves indicated that the initial cAMP peak observed in β-arr DKO cells is slightly more prolonged when compared with that observed in parental wild-type cells (Extended Data Fig. 5b and Supplementary Table 1). Nevertheless, the initial cAMP peak measured in β-arr DKO cells still obviously decayed, with β-arr1/2 depletion slowing the decay time constant only by ~2-fold. This indicates that a second, β-arrestin-independent mechanism for terminating the initial VIPR1 signaling peak must exist.

https://doi.org/10.1038/s41589-023-01412-4

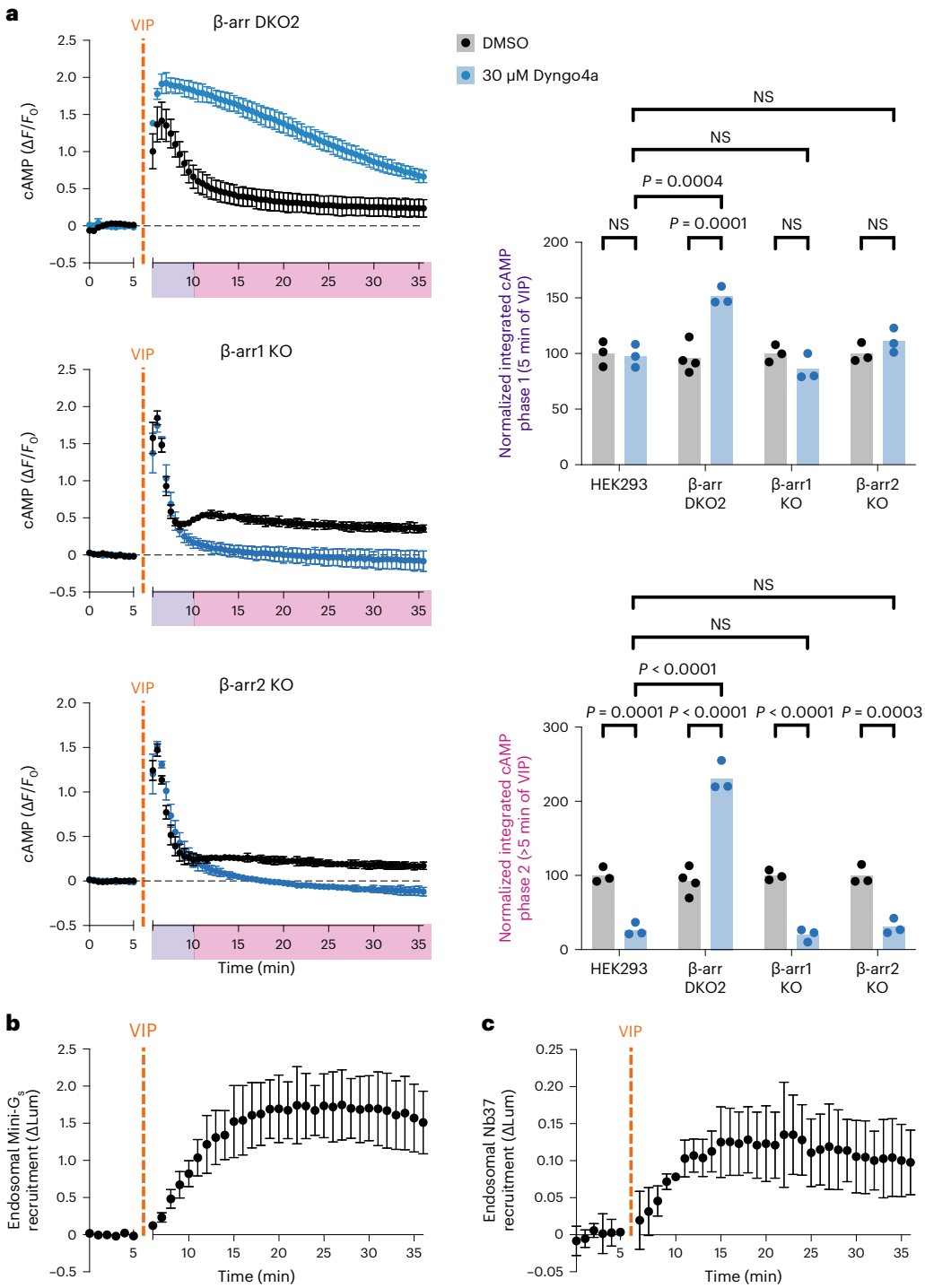

Fig. 3 | β-arrestin is dispensable for VIPR1 endosomal cAMP signaling. a, Changes in cAMP in β-arr1/2 DKO line (β-arr DKO2) and β-arr1/2 single KO lines (β-arr1 KO and β-arr2 KO) upon treatment with 500 nM VIP added at 5 min. Cells were pretreated with 30 μM Dyngo4a (blue) or DMSO (black) for 10 min. Integrated cAMP of each phase (0–5 min or 5–30 min of VIP treatment) was calculated as the area under the curve and normalized to the average DMSO value for each cell line. Data for WT HEK293 are repeated from Fig. 2a. Significance was determined by a two-way ANOVA with Tukey's multiple comparisons test along with data for β-arr DKO1 cell line shown in Extended Data Fig. 5a. $n = 3–4$, as indicated in integrated cAMP plots. **b**,**c**, NanoBiT bystander assays in β-arr DKO2 cells showing endosomal recruitment of mini-G_s (**b**, $n = 3$) or Nb37 (**c**, $n = 4$) upon addition of 1 μM VIP at 5 min. For all panels, data represent biological replicates and are shown as individual data points or mean ± s.d.

We found that imposing endocytic blockade with Dyngo4a dramatically prolonged the VIP-induced cAMP elevation measured in β-arr DKO cells (Fig. 3a, Extended Data Fig. 5a and Supplementary Table 1), in contrast to its much smaller effect in wild-type cells. This indicates that endocytosis by itself can terminate the initial VIPR1-mediated cAMP elevation in cells lacking β-arrestin. That endocytosis itself can attenuate the first cAMP peak without β-arrestin is fully consistent with β-arrestin-independent internalization of VIPR1, and it suggests that endocytosis and β-arrestin semiredundantly terminate the first cAMP peak in wild-type cells.

https://doi.org/10.1038/s41589-023-01412-4

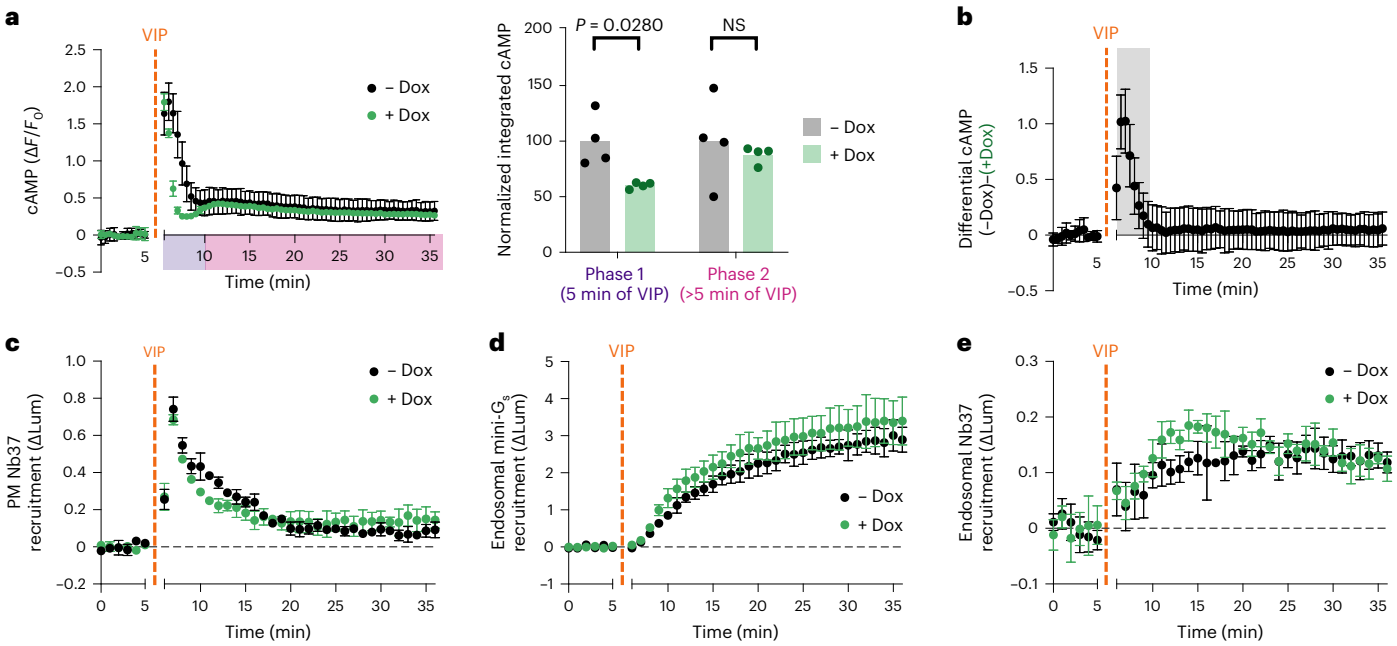

Fig. 4 | β-arrestin resolves phases of cAMP signaling. a, Changes in cAMP in β-arr DKO2-R with (green) and without (black) Dox induction upon treatment with 500 nM VIP added at 5 min. Integrated cAMP of each phase (0–5 min or 5–30 min of VIP treatment) was calculated as the area under the curve and normalized to the average −Dox value. Significance was determined by a repeated measures two-way ANOVA with Sidak's multiple comparisons test along with data for DKO1-R shown in Extended Data Fig. 7a. $n = 4$. **b**, Difference in cAMP response with and without β-arr2 expression, calculated as the difference between the −Dox and +Dox curves shown in **a**. Shaded area represents timepoints where the difference is statistically significant, as determined by a repeated measures two-way ANOVA ($P < 0.05$) with Sidak's multiple comparisons test carried out on the curves in **a**. **c**–**e**, NanoBiT bystander assays showing plasma membrane recruitment of Nb37 (**c**, $n = 3$) or endosomal recruitment of mini-G_s (**d**, $n = 3$) or Nb37 (**e**, $n = 4$) in β-arr DKO2-R cells upon addition of 1 μM VIP at 5 min. For all panels, cells treated with Dox to induce expression of β-arr2-mApple are shown in green, and data represent biological replicates, shown as individual data points or mean ± s.d.

β-arr1 and β-arr2 are both endogenously expressed in HEK293 cells[38] and, while we observed similar recruitment of each isoform to activated VIPR1 (Fig. 1e,f), we wondered whether the signal-attenuating effect might be unique to one isoform. To explore this question, we measured VIP-induced cAMP signaling in β-arrestin single KO cell lines (Extended Data Fig. 5c,d). In cells selectively deficient in β-arr1 or β-arr2, VIP application elicited cAMP elevation similar in kinetics to that observed in wild-type cells (Fig. 3a and Supplementary Table 1). Importantly, in both single KO cell backgrounds, VIPR1 desensitization was observed upon endocytic inhibition, and blocking endocytosis reduced the second phase of signaling to a degree comparable to the reduction observed in wild-type cells (Fig. 3a). Therefore, both β-arrestins appear similar in their overall effects on VIPR1 cAMP signaling as assessed with the present methods.

While we did not observe a distinct, second cAMP peak in β-arr DKO cells, a plateau above baseline was still observed (Fig. 3a). This contrasts with a complete loss of the cAMP plateau produced by endocytic inhibition in wild-type cells (Figs. 2a and 3a and Extended Data Fig. 5a). Further, VIP-induced endosomal recruitment of both mini-G_s and Nb37 was still observed in β-arr DKO cells (Fig. 3b,c and Extended Data Fig. 5e,f). Together, these results indicate that β-arrestin is not required for VIPR1 to initiate either the plasma membrane or endosomal phases of G_s activation or cAMP elevation.

β-Arrestin temporally resolves the VIPR1 signaling phases

If β-arrestin binds active VIPR1 but is not necessary for receptor trafficking or signaling, then what role does it play in modulating VIPR1 activity? That the β-arr DKO cell lines displayed a broader, Dyngo4a-sensitive cAMP peak compared with the sharply biphasic cAMP production in parental cells suggested that β-arrestin sculpts response kinetics. To more precisely investigate this, we pursued genetic rescue in β-arr DKO cells using recombinant β-arr2 (β-arr2-mApple) expressed under tetracycline-inducible control (DKO-R, Extended Data Fig. 6). As expected, a comparison of real-time cAMP dynamics in these cells indicated that overexpression of β-arr2 (+Dox) accelerates the desensitization of the first phase of VIP-induced cytoplasmic cAMP elevation relative to the uninduced (−Dox) condition (Fig. 4a,b and Extended Data Fig. 7a,b). We further quantified this effect by fitting decay constants to the desensitization of the first phase, which showed around a twofold increase upon β-arr2 induction (Supplementary Table 1), as well as by calculating the first derivative of the curves, which became more negative upon β-arr2 induction (Extended Data Fig. 7c). While we observed a subtle corresponding decrease in Nb37 recruitment to the plasma membrane upon β-arr2 induction, this trend was not statistically significant when assessed across the two independent β-arr DKO cell lines (Fig. 4c and Extended Data Fig. 7d).

Some GPCRs that bind β-arrestin in endosomes use this interaction to potentiate cAMP signaling[2,11,24–28]. However, the cellular cAMP elevation observed during the plateau phase of VIPR1 signaling was not detectably affected by β-arr2 overexpression, and the only statistically significant difference in the cAMP elevation with or without β-arr2 overexpression occurred in the first 5 min after VIP application (Fig. 4a,b and Extended Data Fig. 7a,b). This observation indicates that β-arrestin, despite attenuating the plasma membrane signaling phase, does not detectably modulate the endosomal cAMP signaling phase either positively or negatively. We returned to the NanoBiT bystander assays to explore this further. In agreement with the bulk cAMP assays, neither mini-G_s nor Nb37 recruitment to the endosome was markedly altered by β-arr2 overexpression in the two β-arr DKO cell lines tested (Fig. 4d,e and Extended Data Fig. 7e,f).

Together, these data verify that β-arrestin is not necessary for VIPR1-mediated signaling from endosomes and indicate that β-arrestin

https://doi.org/10.1038/s41589-023-01412-4

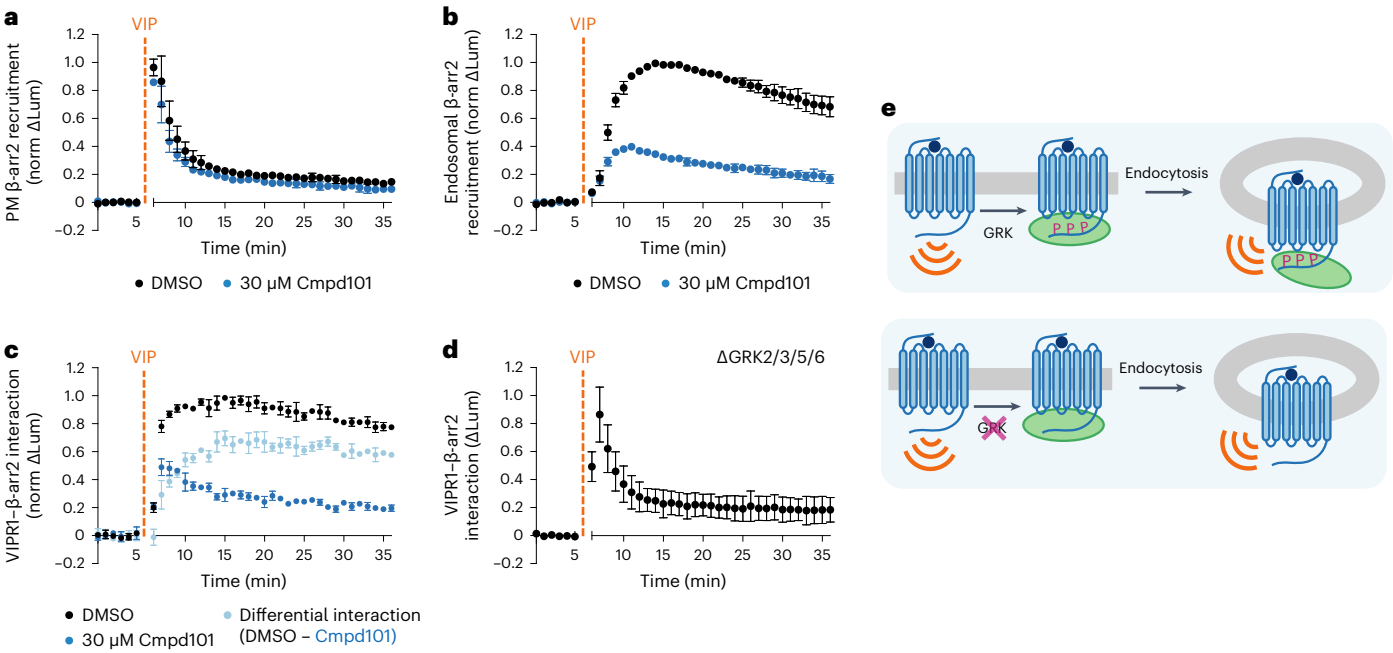

Fig. 5 | VIPR1–β-arrestin complexes at the plasma membrane and endosomes are differentially regulated by GRKs. a,**b**, NanoBiT bystander assays showing plasma membrane (**a**) or endosomal (**b**) recruitment of β-arr2 in HEK293 cells upon addition of 1 μM VIP at 5 min. Cells were pretreated with DMSO (black) or 30 μM Cmpd101 (blue) for 10 min. **c**,**d**, Direct NanoBiT assay showing recruitment of β-arr2 to VIPR1 in HEK293 (**c**) or HEK293A GRK2/3/5/6 KO cells (**d**) upon addition of 1 μM VIP at 5 min. HEK293 cells were pretreated with DMSO (black) or 30 μM Cmpd101 (blue) for 10 min. The light blue curve in **c** represents the difference in interaction over time due to Cmpd101, calculated as the difference between the DMSO and Cmpd101 curves. **e**, Model for GRK regulation of VIPR1–β-arrestin complexes. Upon VIP stimulation, VIPR1 is phosphorylated by GRKs, leading to the recruitment of β-arrestin to VIPR1 at both the plasma membrane and endosomes. If VIPR1 phosphorylation by GRKs is blocked, β-arrestin is still recruited to VIPR1 at the plasma membrane, but a VIPR1–β-arrestin complex does not form at the endosome. For all panels, data represent three biological replicates shown as mean ± s.d. Norm ΔLum, normalized change in luminescence.

binding differentially modulates VIPR1 signaling activity depending on the subcellular location of the complex. The net effect of this selective modulation, with β-arrestin complex formation at the plasma membrane being signal-attenuating and at endosomes being signaling-neutral, is to cause the plasma membrane and endosomal signaling phases to resolve as separate cAMP peaks. Accordingly, β-arrestin's primary function in VIPR1 signaling appears to be to convert distinct phases of VIPR1-Gs activation that are initiated from spatially resolved subcellular locations into temporally resolved phases of global cytoplasmic cAMP elevation.

Location-specific differences in VIPR1–β-arrestin complexes

Our data using the β-arr DKO rescue cell lines indicate that VIPR1–β-arrestin complexes are functionally different depending on their subcellular localization. To begin to investigate the biochemical underpinnings of these functional differences, we explored how GRK-mediated phosphorylation of VIPR1 affects complex formation at the plasma membrane and endosomes. Chemical inhibition of GRK2/3 in HEK293 cells using Compound 101 (Cmpd101) (ref. 44) did not substantially affect VIP-stimulated recruitment of β-arr2 to the plasma membrane, but it strongly inhibited recruitment to endosomes (Fig. 5a,b). This differential effect of Cmpd101 on β-arrestin recruitment elicited by VIPR1 at each membrane location stands in contrast to recruitment of β-arrestin by V2R, a GPCR that also binds β-arrestin at both locations[11,45]. For the V2R, Cmpd101 markedly inhibited β-arr2 recruitment at both the plasma membrane and endosomes (Extended Data Fig. 8a,b). The selective effect on endosomal recruitment of β-arrestin was not due to a lack of VIPR1 internalization, as Cmpd101 had no effect on the agonist-induced endocytosis of VIPR1 (Extended Data Fig. 8c). Further, a direct NanoBiT assay examining the time course of VIPR1–β-arr2 binding indicated that complex sensitivity to Cmpd101 is itself location-dependent, with observed inhibition increasing at later timepoints (>5 min of VIP) that correspond to when receptors are present in endosomes (Fig. 5c). Providing genetic confirmation of this pharmacological result, VIPR1–β-arr2 complexes were rapidly formed but transient in ΔGRK2/3/5/6 cells[46] (Fig. 5d). Together, these results suggest that VIPR1–β-arrestin complex formed at the plasma membrane differs biochemically from that formed at the plasma membrane. The VIPR1–β-arrestin complex that terminates signaling at the plasma membrane does not require GRK-mediated phosphorylation of receptors to form. The complex present on the endosome limiting membrane that is signaling-neutral, in marked contrast, is specifically GRK-dependent (Fig. 5e).

Discussion

The present findings take advantage of the distinct trafficking properties of VIPR1 to disentangle the effects of β-arrestin and endocytosis on the G_s-coupled cellular cAMP response elicited by this GPCR. By doing so, our results establish VIPR1 as a GPCR that is capable of internalizing and initiating a second phase of endosomal G_s-cAMP signaling in the complete absence of β-arrestin. We further show that β-arrestin plays a different role in determining the cellular VIPR1 response by resolving the plasma membrane and endosome signaling phases into separate and sequential global cAMP peaks. We note that a number of GPCRs internalize in a β-arrestin-independent manner[23,30], and some, such as the glucagon-like peptide-1 receptor (GLP1R), have separately been shown to signal from endosomes[14]. However, to our knowledge, the present results are the first to explicitly show, for any GPCR, generation of an endosomal G_s-cAMP signal in the complete absence of cellular β-arrestin.

Accordingly, we propose to revise the present concept of endosomal signaling by GPCRs and, in particular, expand the understanding of how receptor interactions with β-arrestin impact the spatiotemporal profile of cAMP signaling (Fig. 6). For receptors that weakly bind

https://doi.org/10.1038/s41589-023-01412-4

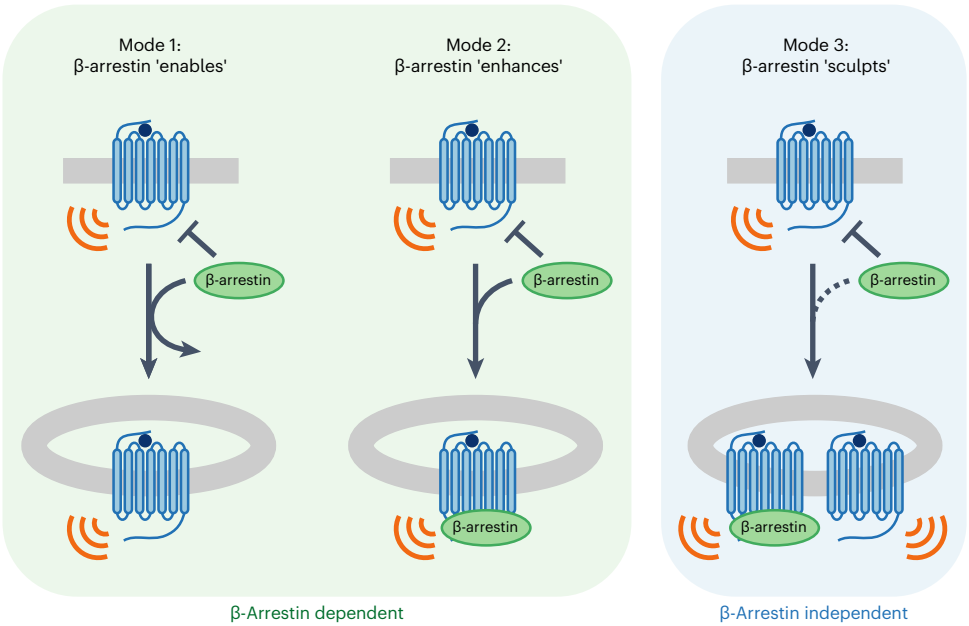

Fig. 6 | VIPR1 defines a third mode of endosomal GPCR signaling. The diagram illustrates key distinctions among signaling modes. Mode 1: β-arrestin enables signaling from endosomes by promoting receptor internalization and then dissociating. Mode 2: β-arrestin promotes receptor internalization and then remains bound after internalization to form a signal-sustaining endosomal megaplex. Mode 3: β-arrestin is not required for receptor internalization or signaling from endosomes; instead, β-arrestin sculpts the resulting combined signal output, such that the plasma membrane and endosomal signal phases produce temporally resolved cAMP peaks.

β-arrestin, exemplified by the TSHR, β-arrestin enables signaling to occur from endosomes by promoting receptor internalization before dissociating[9,47]. For some receptors that more strongly bind β-arrestin, exemplified by PTHR1 and V2R, β-arrestin enhances the endosomal signal by remaining bound to form a signal-boosting complex specifically on the endosome membrane[2,24–26,28]. In the case of VIPR1, β-arrestin is not required to generate the endosomal signal. Rather, it sculpts receptor activity such that sequential peaks of receptor/G protein activation initiated from different subcellular locations—the plasma membrane and endosomes—are resolved into temporally separated peaks of global cytoplasmic cAMP elevation. As β-arrestin is not needed even to deliver receptors to the endosome, this third mode of endosomal signaling reveals a discrete function of β-arrestin in regulating the spatiotemporal profile of the integrated cellular cAMP signal. Because other GPCRs have been reported to internalize independently of β-arrestin[23,30], we anticipate that the additional endosomal signaling mode and β-arrestin function revealed in the present study is not unique to VIPR1 and likely underlies GPCR-specific modulation of cellular signaling more broadly.

β-Arrestin mediates this signal-sculpting function by selectively accelerating the rate at which the plasma membrane signaling phase is attenuated while having little or no effect on the endosomal signaling phase. The mechanistic basis for this specificity in β-arrestin function appears to be the presence of distinct GPCR–β-arrestin complexes at the plasma membrane relative to at the endosome limiting membrane, as established here by differences in their dependence on GRK-mediated receptor phosphorylation for formation or stability. This supports the emerging view that GPCR–β-arrestin complexes dynamically remodel during endocytic trafficking to enable location-specific control[25,28,29,48,49].

Further investigation will be needed to determine the biophysical basis for this biochemical distinction. Transition from a 'core-engaged' GPCR–β-arrestin complex to a 'tail-engaged' complex is thought to underlie the ability of β-arrestin to switch from a signal-attenuating factor at the plasma membrane to a signal-enhancing factor at the endosome for receptors such as PTHR[25,28,29]. Therefore, a simple model is that the signal-attenuating VIPR1–β-arrestin complex formed at the plasma membrane corresponds to a receptor 'core-engaged' complex that can form in the absence of a phosphorylated receptor tail, while the signaling-neutral VIPR1–β-arrestin complex formed at endosomes corresponds to a phosphorylation-dependent 'tail-engaged' complex (Fig. 5e). While there are examples of signaling-neutral GPCR–β-arrestin mutant complexes that are permissive of G protein signaling without modulating the cAMP response[28], it remains unclear how a signaling-neutral VIPR1–β-arrestin complex may be distinct from previously described 'tail-engaged' signal-enhancing GPCR–β-arrestin complexes. In particular, our data indicate that GRK-mediated phosphorylation is not required for the VIPR1–β-arrestin complex that desensitizes signaling from the plasma membrane. This contrasts with the behavior of other GPCRs that require phosphorylation to recruit β-arrestin, as we verify here for V2R. However, we note that some other GPCRs have been shown to recruit β-arrestin in the absence of phosphorylation (for example, see ref. 50).

In sum, we demonstrate endosomal GPCR signaling in the absence of β-arrestin and the formation of functionally distinct GPCR–β-arrestin complexes at endosomes relative to the plasma membrane. These results point to additional diversity in GPCR–β-arrestin complex formation that enables the functional signaling properties of GPCRs to be precisely tuned in a receptor-specific manner, and according to differences in the posttranslational modification of receptors at discrete membrane locations.

Online content

Any methods, additional references, Nature Portfolio reporting summaries, source data, extended data, supplementary information, acknowledgements, peer review information; details of author contributions and competing interests; and statements of data and code availability are available at https://doi.org/10.1038/s41589-023-01412-4.

References

1. Hauser, A. S., Attwood, M. M., Rask-Andersen, M., Schiöth, H. B. & Gloriam, D. E. Trends in GPCR drug discovery: new agents, targets and indications. *Nat. Rev. Drug Discov.* **16**, 829–842 (2017).
2. Sutkeviciute, I. & Vilardaga, J.-P. Structural insights into emergent signaling modes of G protein–coupled receptors. *J. Biol. Chem.* **295**, 11626–11642 (2020).
3. Hilger, D., Masureel, M. & Kobilka, B. K. Structure and dynamics of GPCR signaling complexes. *Nat. Struct. Mol. Biol.* **25**, 4–12 (2018).
4. Katritch, V., Cherezov, V. & Stevens, R. C. Structure-function of the G protein–coupled receptor superfamily. *Annu. Rev. Pharmacol. Toxicol.* **53**, 531–556 (2013).
5. Weis, W. I. & Kobilka, B. K. The molecular basis of G protein–coupled receptor activation. *Annu. Rev. Biochem.* **87**, 897–919 (2018).
6. Calebiro, D. & Koszegi, Z. The subcellular dynamics of GPCR signaling. *Mol. Cell. Endocrinol.* **483**, 24–30 (2019).
7. Lobingier, B. T. & von Zastrow, M. When trafficking and signaling mix: how subcellular location shapes G protein-coupled receptor activation of heterotrimeric G proteins. *Traffic* **20**, 130–136 (2019).
8. Hanyaloglu, A. C. & Zastrow, Mvon Regulation of GPCRs by endocytic membrane trafficking and its potential implications. *Annu. Rev. Pharmacol. Toxicol.* **48**, 537–568 (2008).
9. Calebiro, D. et al. Persistent cAMP-signals triggered by internalized G-protein–coupled receptors. *PLoS Biol.* **7**, e1000172 (2009).
10. Ferrandon, S. et al. Sustained cyclic AMP production by parathyroid hormone receptor endocytosis. *Nat. Chem. Biol.* **5**, 734–742 (2009).
11. Feinstein, T. N. et al. Noncanonical control of vasopressin receptor type 2 signaling by retromer and arrestin. *J. Biol. Chem.* **288**, 27849–27860 (2013).
12. Irannejad, R. et al. Conformational biosensors reveal GPCR signalling from endosomes. *Nature* **495**, 534–538 (2013).
13. Merriam, L. A. et al. Pituitary adenylate cyclase 1 receptor internalization and endosomal signaling mediate the pituitary adenylate cyclase activating polypeptide-induced increase in guinea pig cardiac neuron excitability. *J. Neurosci.* **33**, 4614–4622 (2013).
14. Kuna, R. S. et al. Glucagon-like peptide-1 receptor-mediated endosomal cAMP generation promotes glucose-stimulated insulin secretion in pancreatic β-cells. *Am. J. Physiol. Endocrinol. Metab.* **305**, E161–E170 (2013).
15. Lyga, S. et al. Persistent cAMP signaling by internalized LH receptors in ovarian follicles. *Endocrinology* **2016**, 63–71 (2016).
16. Tsvetanova, N. G. & von Zastrow, M. Spatial encoding of cyclic AMP signaling specificity by GPCR endocytosis. *Nat. Chem. Biol.* **10**, 1061–1065 (2014).
17. Godbole, A., Lyga, S., Lohse, M. J. & Calebiro, D. Internalized TSH receptors en route to the TGN induce local Gs-protein signaling and gene transcription. *Nat. Commun.* **8**, 443 (2017).
18. White, A. D. et al. Spatial bias in cAMP generation determines biological responses to PTH type 1 receptor activation. *Sci. Signal.* **14**, eabc5944 (2021).
19. Tsvetanova, N. G. et al. Endosomal cAMP production broadly impacts the cellular phosphoproteome. *J. Biol. Chem.* **297**, 100907 (2021).
20. Jean-Alphonse, F. et al. Spatially restricted G protein-coupled receptor activity via divergent endocytic compartments. *J. Biol. Chem.* **289**, 3960–3977 (2014).
21. Sposini, S. et al. Integration of GPCR signaling and sorting from very early endosomes via opposing APPL1 mechanisms. *Cell Rep.* **21**, 2855–2867 (2017).
22. Gurevich, V. V. & Gurevich, E. V. GPCR signaling regulation: the role of GRKs and arrestins. *Front. Pharmacol.* **10**, 125 (2019).
23. Moo, E. V., van Senten, J. R., Bräuner-Osborne, H. & Møller, T. C. Arrestin-dependent and -independent internalization of G protein–coupled receptors: methods, mechanisms, and implications on cell signaling. *Mol. Pharmacol.* **99**, 242–255 (2021).
24. Feinstein, T. N. et al. Retromer terminates the generation of cAMP by internalized PTH receptors. *Nat. Chem. Biol.* **7**, 278–284 (2011).
25. Thomsen, A. R. B. et al. GPCR-G protein-β-arrestin super-complex mediates sustained G protein signaling. *Cell* **166**, 907–919 (2016).
26. Gidon, A. et al. Endosomal GPCR signaling turned off by negative feedback actions of PKA and v-ATPase. *Nat. Chem. Biol.* **10**, 707–709 (2014).
27. Wehbi, V. L. et al. Noncanonical GPCR signaling arising from a PTH receptor–arrestin–Gβγ complex. *Proc. Natl Acad. Sci. USA* **110**, 1530–1535 (2013).
28. Cahill, T. J. et al. Distinct conformations of GPCR–β-arrestin complexes mediate desensitization, signaling, and endocytosis. *Proc. Natl Acad. Sci. USA* **114**, 2562–2567 (2017).
29. Nguyen, A. H. et al. Structure of an endosomal signaling GPCR–G protein–β-arrestin megacomplex. *Nat. Struct. Mol. Biol.* **26**, 1123–1131 (2019).
30. Claing, A. et al. Multiple endocytic pathways of G protein-coupled receptors delineated by GIT1 sensitivity. *Proc. Natl Acad. Sci. USA* **97**, 1119–1124 (2000).
31. Shetzline, M. A., Walker, J. K. L., Valenzano, K. J. & Premont, R. T. Vasoactive intestinal polypeptide type-1 receptor regulation. *J. Biol. Chem.* **277**, 25519–25526 (2002).
32. Jonker, C. T. H. et al. Accurate measurement of fast endocytic recycling kinetics in real time. *J. Cell Sci*. https://doi.org/10.1242/jcs.231225 (2019).
33. Langlet, C. et al. Contribution of the carboxyl terminus of the VPAC1 receptor to agonist-induced receptor phosphorylation, internalization, and recycling. *J. Biol. Chem.* **280**, 28034–28043 (2005).
34. Gee, H. Y. et al. Synaptic scaffolding molecule binds to and regulates vasoactive intestinal polypeptide type-1 receptor in epithelial cells. *Gastroenterology* **137**, 607–617.e4 (2009).
35. Xu, Z. et al. Structural basis of sphingosine-1-phosphate receptor 1 activation and biased agonism. *Nat. Chem. Biol.* **18**, 281–288 (2022).
36. Eneman, B. et al. Distribution and function of PACAP and its receptors in the healthy and nephrotic kidney. *Nephron* **132**, 301–311 (2016).
37. Atwood, B. K., Lopez, J., Wager-Miller, J., Mackie, K. & Straiker, A. Expression of G protein-coupled receptors and related proteins in HEK293, AtT20, BV2, and N18 cell lines as revealed by microarray analysis. *BMC Genomics* **12**, 14 (2011).
38. Cho, N. H. et al. OpenCell: endogenous tagging for the cartography of human cellular organization. *Science* **375**, eabi6983 (2022).
39. Holtmann, M. H., Hadac, E. M. & Miller, L. J. Critical contributions of amino-terminal extracellular domains in agonist binding and activation of secretin and vasoactive intestinal polypeptide receptors. Studies of chimeric receptors. *J. Biol. Chem.* **270**, 14394–14398 (1995).
40. Tasma, Z. et al. Characterisation of agonist signalling profiles and agonist-dependent antagonism at PACAP-responsive receptors: implications for drug discovery. *Br. J. Pharmacol.* **179**, 435–453 (2022).
41. Carpenter, B. & Tate, C. G. Engineering a minimal G protein to facilitate crystallisation of G protein-coupled receptors in their active conformation. *Protein Eng. Des. Sel.* **29**, 583–594 (2016).

42. Wan, Q. et al. Mini G protein probes for active G protein–coupled receptors (GPCRs) in live cells. *J. Biol. Chem.* **293**, 7466–7473 (2018).
43. Westfield, G. H. et al. Structural flexibility of the Gαs α-helical domain in the β_2-adrenoceptor Gs complex. *Proc. Natl Acad. Sci. USA* **108**, 16086–16091 (2011).
44. Thal, D. M., Yeow, R. Y., Schoenau, C., Huber, J. & Tesmer, J. J. G. Molecular mechanism of selectivity among G protein-coupled receptor kinase 2 inhibitors. *Mol. Pharmacol.* **80**, 294–303 (2011).
45. Oakley, R. H., Laporte, S. A., Holt, J. A., Barak, L. S. & Caron, M. G. Association of β-arrestin with G protein-coupled receptors during clathrin-mediated endocytosis dictates the profile of receptor resensitization. *J. Biol. Chem.* **274**, 32248–32257 (1999).
46. Kawakami, K. et al. Heterotrimeric Gq proteins act as a switch for GRK5/6 selectivity underlying β-arrestin transducer bias. *Nat. Commun.* **13**, 487 (2022).
47. Frenzel, R., Voigt, C. & Paschke, R. The human thyrotropin receptor is predominantly internalized by β-arrestin 2. *Endocrinology* **147**, 3114–3122 (2006).
48. Janetzko, J. et al. Membrane phosphoinositides regulate GPCR-β-arrestin complex assembly and dynamics. *Cell* **185**, 4560–4573.e19 (2022).
49. Shukla, A. K. et al. Visualization of arrestin recruitment by a G-protein-coupled receptor. *Nature* **512**, 218–222 (2014).
50. Drube, J. et al. GPCR kinase knockout cells reveal the impact of individual GRKs on arrestin binding and GPCR regulation. *Nat. Commun.* **13**, 540 (2022).

Methods

Cell culture

HEK293 (ATCC CRL-1573) and HEK239A ΔGRK2/3/5/6 (ref. 46) were cultured in DMEM (Gibco 1196511) supplemented with 10% FBS (Hyclone SH30910.03). Besides ΔGRK2/3/5/6, all other KO and stable cell lines used in this study were derived from the HEK293 cell line. Cells stably expressing FLAG-VIPR1 (CMV) were selected using 500 μg ml^{-1} geneticin, and cells stably expressing HaloTag-VIPR1 (CMV) or HaloTag-β2AR were selected using 25 μg ml^{-1} zeocin. Cell lines stably expressing tet-inducible (TRE3G) HaloTag-VIPR1 or β-arr2-mApple were selected using 2 μg ml^{-1} puromycin and screened for inducible expression by flow cytometry. Rescue was induced 24 h before experiments using 1 μg ml^{-1} doxycycline. All cells were routinely checked for mycoplasma contamination (MycoAlert, Lonza).

DNA constructs

Information on all plasmids used in this study can be found in Supplementary Table 2. Lipofectamine 2000 (Thermo Fisher) was used for transfections according to the manufacturer's protocol. BacMam from pCMV-Dest constructs was produced according to the manufacturer's protocol.

Generation of CRISPR KO cell lines

Single guide RNAs (sgRNAs) (Supplementary Table 3) were designed using the Synthego CRISPR design tool. To make ribonucleoprotein (RNP), 3 μl total of 53.3 μM sgRNA (Synthego) was mixed with 2 μl of 40 μM Cas9 (UC Berkeley Macrolab), and the mixture was incubated at room temperature for 10 min. Electroporation of the RNP complex was carried out using the SF Cell Line 4D-Nucleofector kit (Lonza) and program CM-130 with 2.0×10^5 cells. Genetic modifications of monoclonal cell lines were verified from genomic PCR amplicons (Supplementary Tables 3 and 4) using Sanger sequencing in combination with the Synthego ICE Analysis Tool or by next-generation sequencing (Amplicon-EZ, Azenta Life Sciences). β-arr1/2 expression was assessed by western blot using the antibodies listed in Supplementary Table 5. Western blots were imaged on an Odyssey Imager (v.2.0.3, LI-COR Biosciences) and quantified using Fiji (v.1.53) (ref. 51). For the β-arr DKO1 cell line, ARRB1 and ARRB2 modifications were done simultaneously, while for the β-arr DKO2 cell line, modifications were done sequentially.

cADDis microplate cAMP assay

Real-time intracellular cAMP was measured using the Green Up cADDis cAMP biosensor (Montana Molecular), as described previously[52]. Briefly, cells were treated with cADDis BacMam and plated into 96-well plates (Corning 3340). After 24 h, cells were washed with assay buffer (20 mM HEPES pH 7.4, 135 mM NaCl, 5 mM KCl, 0.4 mM $MgCl_2$, 1.8 mM $CaCl_2$, 5 mM D-glucose) twice before a 10-min incubation in a 37 °C plate reader (Synergy H4, Gen5 v.2.05, BioTek), optionally with DMSO or Dyngo4a (30 μM, Abcam ab120689) as indicated in figure legends. Fluorescence was read at an excitation wavelength of 500 nm and an emission wavelength of 530 nm every 20–30 s for 35 min, with vehicle or agonist added after 5 min. Change in intracellular cAMP ($\Delta F/F_0$) was calculated as the change in fluorescence ($\Delta F = F - F_0$) normalized to the average of the 5-min baseline (F_0). For dose–response curves, peak cAMP values, normalized to the average peak response to 1 μM PACAP, were fit to the equation: $\text{peak cAMP} = \frac{100 \times [\text{Agonist}]}{EC_{50} - [\text{Agonist}]}$.

cADDis live epifluorescence microscopy

Cells were transfected with the appropriate constructs 48 h before experiments and plated into glass-bottom dishes (MatTek Corporation) coated with 0.001% (w/v) poly-L-lysine (Millipore Sigma). Cells were washed three times with assay media (DMEM, no phenol red, 30 mM HEPES pH 7.4) before imaging. Imaging was conducted using a Nikon TE2000 inverted microscope fitted with a Nikon ×20/0.7 numerical aperture objective, Sutter Lambda HPX-L5 LED epifluorescence illuminator, Sutter excitation/emission filter wheels and Point Grey CMOS camera controlled by Micromanager v.1.4.23 (ref. 53) (www.micro-manager.org). A dual-channel dichroic filter set (Chroma 89021) was used to separately acquire cADDis (470/40 excitation, 520/50 emission) and mCherry (572/35 excitation, 632/60 emission) fluorescence signals. Cells were maintained at 37 °C during image collection using a custom-built heated stage and stage-top incubator. Then, 1 μM VIP was added after a 2-min baseline, and forskolin (Fsk, 10 μM, Millipore Sigma) and 3-isobutyl-1-methylxanthine (IBMX, 500 μM, Millipore Sigma) were added 30 min later. Data were processed using Cell Profiler 4 (ref. 54) (www.cellprofiler.org). Briefly, cells were identified using the mCherry channel, and the intensity of the cADDis channel was measured over the entire image and in the cell mask. Each frame was background-corrected by subtracting the lower quartile fluorescence intensity of the entire image. The normalized change in fluorescence of the cell mask was calculated as $(F - F_0)/(F_{\text{FskIBMX}} - F_0)$, where F_0 is the average fluorescence over the first 2 min and F_{FskIBMX} is the average fluorescence of the final 2 min. Each biological replicate is the average of 1–2 dishes of approximately 20–30 cells per dish.

NanoBiT luciferase complementation assays

Cells grown in six-well plates were transfected with receptor (HaloTag-VIPR1 or FLAG-V2R) and the appropriate LgBit/SmBiT constructs 24 h before experiments. Experiments using Nb37-SmBiT(114) (Fig. 4c and Extended Data Fig. 7d) or Nb37-SmBiT(101) (all other figures) also required the cotransfection of a tricistronic G protein construct (human Gβ1, bovine Gγ1 and human Gαs). For the assay, cells were lifted and centrifuged at 500*g* for 3 min. Cells were resuspended in assay buffer supplemented with 5 μM coelenterazine-H (Research Products International) to a concentration of 5×10^5 or 1×10^6 cells per ml, and 100 μl of cells were plated into untreated white 96-well plates (Corning 3912). Plates were incubated at 37 °C and 5% CO_2 for 10 min before the assay, optionally with DMSO or Cmpd101 (30 μM, HelloBio HB2840) as indicated in figure legends. Luminescence was read on a plate reader (Synergy H4, Gen5 v.2.05, BioTek) prewarmed to 37 °C. After a 5-min baseline reading, vehicle or agonist were added at concentrations indicated in figure legends, and luminescence was read for another 30 min. To calculate the change in luminescence, each well was first normalized to its average baseline luminescence, and the average change in luminescence for vehicle-treated samples was subtracted from the average change in luminescence for drug-treated samples ($\Delta\text{Lum} = \text{Lum}_{\text{VIP}} - \text{Lum}_{\text{vehicle}}$). To compare DMSO- and Cmpd101-treated samples, readings were further normalized to the maximum ΔLum of the DMSO-treated sample (norm ΔLum).

Confocal microscopy

All fixed and live confocal imaging was carried out using a Nikon Ti inverted microscope controlled by NIS Elements HC v.5.21.03 (Nikon) and fitted with a CSU-22 spinning disk unit (Yokogawa), custom laser launch (100 mW at 405, 488, 561 and 640 nm, Coherent OBIS), Sutter emission filter wheel and Photometrics Evolve Delta EMCCD camera. Samples were imaged using an Apo TIRF ×100/1.49 numerical aperture oil objective (Nikon).

For live imaging, cells were transfected with the appropriate constructs 48 h before experiments and plated into glass-bottom dishes (Cellvis) coated with 0.001% (w/v) poly-L-lysine (Millipore Sigma). For surface labeling of receptor, cells were incubated with either monoclonal anti-FLAG M1 antibody (Millipore Sigma F3040) labeled with Alexa Fluor 647 (Thermo Fisher A20186) or 200 nM JF_{635}i-HTL (ref. 32) for 10 min at 37 °C and 5% CO_2. After three washes, cells were imaged in assay media (DMEM, no phenol red, 30 mM HEPES pH 7.4) in a temperature- and humidity-controlled chamber (Okolab). For time-lapse, cells were imaged at 20-s intervals for 22 min, with 500 nM VIP added after 2 min.

For fixed imaging, cells were transfected with the appropriate constructs 48 h before experiments and plated onto coverslips (Fisher Scientific 12-545-100P) coated with 0.001% (w/v) poly-L-lysine (Millipore Sigma). Coverslips were washed with assay media (DMEM, no phenol red, 30 mM HEPES pH 7.4) and labeled with 200 nM JF_{635}i-HTL for 10 min at 37 °C and 5% CO_2. Vehicle or 500 nM VIP was added for 20 min, followed by washes with PBS and fixation in 3.7% formaldehyde (Fisher, F79) in modified BRB80 (80 mM PIPES pH 6.8, 1 mM $MgCl_2$, 1 mM $CaCl_2$) for 20 min. For immunofluorescence, cells were permeabilized with 0.1% Triton-X100 in 3% BSA before incubation with primary and secondary antibodies as described in Supplementary Table 5. Coverslips were mounted on glass slides using ProLong Gold Antifade mounting medium (Invitrogen P10144).

All image analysis was carried out in Cell Profiler 4 (ref. 54), and all images for figures were processed using Fiji (v.1.53) (ref. 51). For colocalization analysis, the Pearson's correlation coefficient was calculated in individual cells segmented manually.

Receptor internalization by flow cytometry

All experiments were carried out using cell lines stably expressing an N-terminal HaloTag fusion of the receptor of interest. Unless otherwise noted, all experiments used HaloTag-VIPR1 under the control of an inducible promoter (TRE3G) in either a VIPR1 KO or β-arr1/2 DKO cell background. For experiments using mCherry and mCherry-Dyn1K44E, cells were incubated with BacMam for 24 h before the experiment. Agonist or vehicle was added to cells grown in 12-well plates coated with 0.001% (w/v) poly-L-lysine (Millipore Sigma) and incubated at 37 °C and 5% CO_2 as indicated in figure legends. At the end of the incubation, plates were cooled on ice for 10 min, and all subsequent steps were carried out on ice. Cells were then labeled with 200 nM JF_{635}i-HTL for 30 min. After washing once with PBS-EDTA (UCSF Cell Culture Facility), cells were lifted with 100 µl of TrypLE Express (Thermo Fisher) at room temperature for 10 min. TrypLE was quenched with 150 µl of PBS-EDTA + 2.5% FBS, and resuspended cells were transferred into an untreated black 96-well plate (Corning). Data from 10,000 events were collected on an Attune NxT Flow Cytometer equipped with a CytKick Autosampler and controlled by Attune Cytometric Software v.5.3.2415.0 (Thermo Fisher). JF_{635}i-HTL was measured with a 637-nm excitation laser and a 670/14-nm emission filter, while mCherry was measured with a 561-nm excitation laser and a 620/15-nm emission filter. Data were analyzed using FlowJo v.10.8 software (BD Life Sciences). Populations were gated for cells expressing mCherry, when applicable (Supplementary Fig. 1). Surface receptor was calculated as the normalized median fluorescence (JF_{635}i).

Statistical analysis and reproducibility

All data are shown as individual biological replicates or as a mean ± s.d. from at least three biologically independent experiments. Each biological replicate in the cAMP, NanoBiT and flow cytometry assays represents the average of at least two technical replicates, and all images are representative of at least three biologically independent experiments. Rate constants, derivatives and statistical tests were carried out using Prism (v.8 and v.9, GraphPad) as noted in figure legends.

Reporting summary

Further information on research design is available in the Nature Portfolio Reporting Summary linked to this article.

Data availability

Source data are provided with this paper.

References

51. Schindelin, J. et al. Fiji: an open-source platform for biological-image analysis. *Nat. Methods* **9**, 676–682 (2012).
52. Dai, S. A. et al. State-selective modulation of heterotrimeric Gαs signaling with macrocyclic peptides. *Cell* **185**, 3950–3965.e25 (2022).
53. Edelstein, A. D. et al. Advanced methods of microscope control using μManager software. *J. Biol. Methods* **1**, e10 (2014).
54. Stirling, D. R. et al. CellProfiler 4: improvements in speed, utility and usability. *BMC Bioinformatics* **22**, 433 (2021).

Acknowledgements

We thank D. Gordon and A. Ehrlich for assistance with CRISPR; L. Lavis for discussion and sharing reagents; A. Inoue, G. Schulte, R. Irannejad and A. Marley for sharing reagents; B. Barsi-Rhyne and the rest of the von Zastrow laboratory for discussion; and the following core facilities for providing services to support this research: the UCSF Center for Advanced Light Microscopy (K. Herrington, S. Kim and D. Larsen), the UCSF Center for Advanced Technology (E. Chow) and the UCSF Helen Diller Family Comprehensive Cancer Center Laboratory for Cell Analysis (S. Elmes; supported by the National Institutes of Health under award no. P30CA082103). These studies were supported by grants from the National Institutes of Health National Cancer Institute (grant no. F32CA260118 to E.E.B.), National Institute on Drug Abuse (grant nos. DA010711 and DA012864 to M.v.Z.) and National Institute of Mental Health (grant no. MH120212 to M.v.Z.).

Author contributions

E.E.B. and M.v.Z. conceived of and designed the research. E.E.B. carried out experiments. E.E.B. and M.v.Z. analyzed data and wrote the paper.

Competing interests

The authors declare no competing interests.

Additional information

Extended data is available for this paper at https://doi.org/10.1038/s41589-023-01412-4.

Supplementary information The online version contains supplementary material available at https://doi.org/10.1038/s41589-023-01412-4.

Correspondence and requests for materials should be addressed to Mark von Zastrow.

Peer review information *Nature Chemical Biology* thanks Davide Calebiro and the other, anonymous, reviewer(s) for their contribution to the peer review of this work.

https://doi.org/10.1038/s41589-023-01412-4

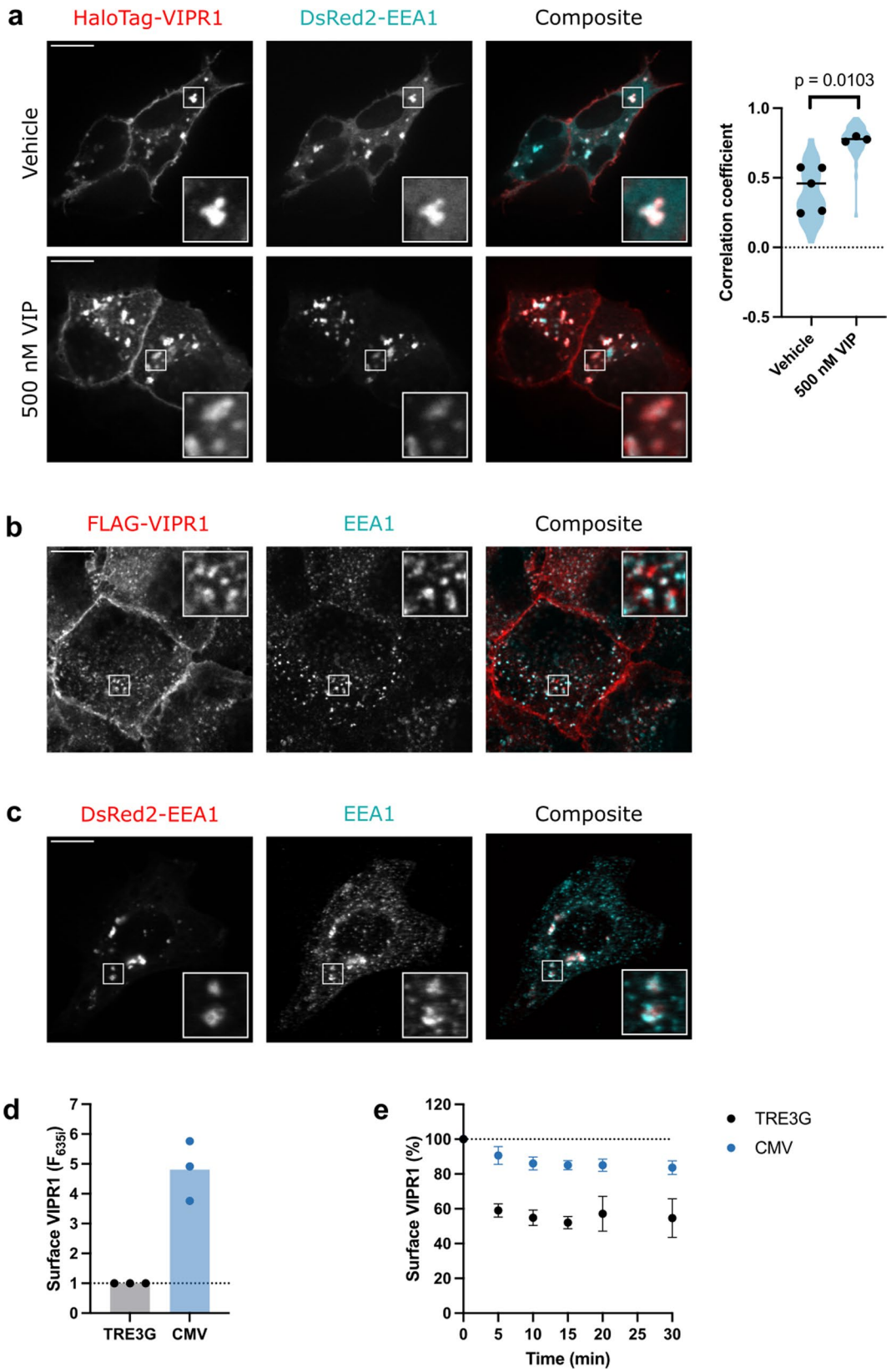

Extended Data Fig. 1 | See next page for caption.

https://doi.org/10.1038/s41589-023-01412-4

Extended Data Fig. 1 | VIPR1 undergoes agonist-induced internalization. **a**, Cells coexpressing HaloTag-VIPR1, labeled with cell-impermeant JF_{635}i-HTL for 10 minutes, and DsRed2-EEA1 were treated with vehicle or 500 nM VIP for 15 minutes before fixation and imaging. Scale bar is 10 µm. For quantification, cells were manually segmented, and the correlation coefficient was calculated for each cell. Mean correlation coefficients are shown for each biological replicate (9–27 cells), with a line at the mean of means and cell-level data superimposed as a violin plot. Significance was determined by an unpaired two-sided t-test. **b**, Representative image (n = 3) showing colocalization of FLAG-VIPR1 and endogenous EEA1 after a 15 minute treatment with 500 nM VIP prior to fixation. Surface FLAG-VIPR1 was labeled with anti-FLAG M1 antibody conjugated to Alexa Fluor 647 for 10 minutes before VIP treatment. Scale bar is 10 µm. **c**, Representative image (n = 2) showing colocalization of overexpressed DsRed-EEA1 and endogenous EEA1. Scale bar is 10 µm. **d**, Comparison of surface HaloTag-VIPR1 levels in cells stably expressing receptor under an inducible (TRE3G, black) or constitutive (CMV, blue) promoter, as measured by flow cytometry. n = 3. **e**, Time course of surface HaloTag-VIPR1 expressed under an inducible (TRE3G, black) or constitutive (CMV, blue) promoter after treatment with 500 nM VIP, as measured by flow cytometry. Data for TRE3G is repeated from Fig. 1b. n = 3. For all panels, data represent biological replicates and are shown as individual data points or mean ± s.d.

https://doi.org/10.1038/s41589-023-01412-4

a

ARRB1 Exon 5

Translation	^{56}T	L	T	C	A	F	R	Y	...	^{72}G	L	T	F	R
Sequence	ACG	CTG	ACC	TGC	GCC	TTC	CGC	TAT	...	GGC	CTG	ACC	TTT	CGC
DKO1 (+1)	ACG	CTG	ACC	TGC	GCC	TTC	CGG	CTA	...	TGG	CCT	GAC	CTT	TCG
DKO1 (-37)	ACG	CTG	ACC	TGC	GCC	T--	---	---	...	---	--G	ACC	TTT	CGC
DKO2 (-48)	ACG	CTG	---	---	---	---	---	---	...	---	---	ACC	TTT	CGC

ARRB2 Intron 4-5 | ARRB2 Exon 5

Translation											^{54}(V)	F	V	T	L	T	C	A	F	R	Y		^{68}D	L
Sequence										CCACTCATCTCACCCTCCCTTGCCAG	TG	TTT	GTG	ACC	CTC	ACC	TGC	GCC	TTC	CGC	TAT	...	GAC	CTG
DKO1 (-39)	CCA----------										--	---	---	---	CTC	ACC	TAC	GGC	---	--C	TAT	...	GAC	CTG
DKO1 (-25)	CCACTCATCTCACCCTCCCTTGCCAG										TG	---	---	---	---	---	---	---	---	-GC	TAT	...	GAC	CTG
DKO1 (-19)	CCACTCATCTCACCCT----------										--	---	---	-CC	CTC	ACC	TGC	GCC	TTC	CGC	TAT	...	GAC	CTG
DKO1 (-5)	CCACTCATCTCACCCTCCCTTG----										T-	TTT	GTG	ACC	CTC	ACC	TGC	GCC	TTC	CGC	TAT	...	GAC	CTG
DKO2 (-40)	CCACTCATCTCACCCTCCCTTGCCAG										TG	---	---	---	---	---	---	---	---	---	---	...	-AC	CTG

b

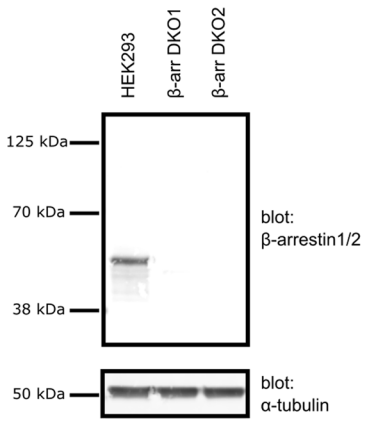

c

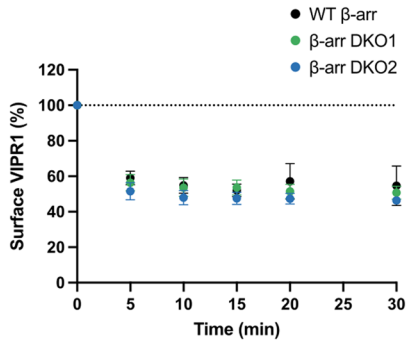

Extended Data Fig. 2 | Characterization of β-arr1/2 DKO CRISPR knockout cell lines used in this study. a, Alignments showing the genetic modifications of β-arr1 (ARRB1) and β-arr2 (ARRB2) in independent monoclonal β-arrestin1/2 double knockout (β-arr1/2 DKO) cell lines. β-arr DKO2 is used for main text figures, while β-arr DKO1 is used for extended data figures. **b**, Representative western blot (n = 3) of parental HEK293 and β-arr1/2 DKO cell lysate, probing for β-arrestin1/2 and α-tubulin as a loading control. **c**, Flow cytometry showing the time course of internalization of HaloTag-VIPR1 in WT (black), β-arr DKO1 (green), β-arr DKO2 (blue) and cells treated with 500 nM VIP. Data for WT β-arr is repeated from Fig. 1b. Data represent three biological replicates shown as mean ± s.d.

https://doi.org/10.1038/s41589-023-01412-4

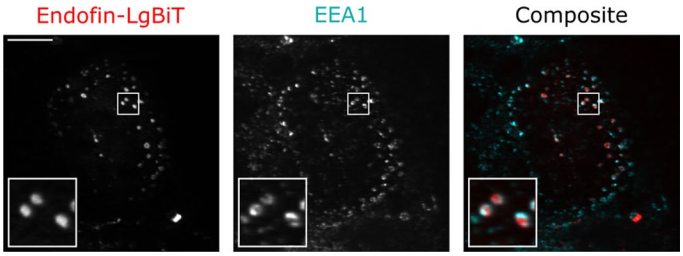

Extended Data Fig. 3 | Endofin-LgBiT and EEA1 localize to an overlapping population of endosomes. Representative image (n = 2) showing overexpressed endofin-LgBiT, stained with an anti-LgBiT antibody, and endogenous EEA1. Scale bar is 10 μm.

https://doi.org/10.1038/s41589-023-01412-4

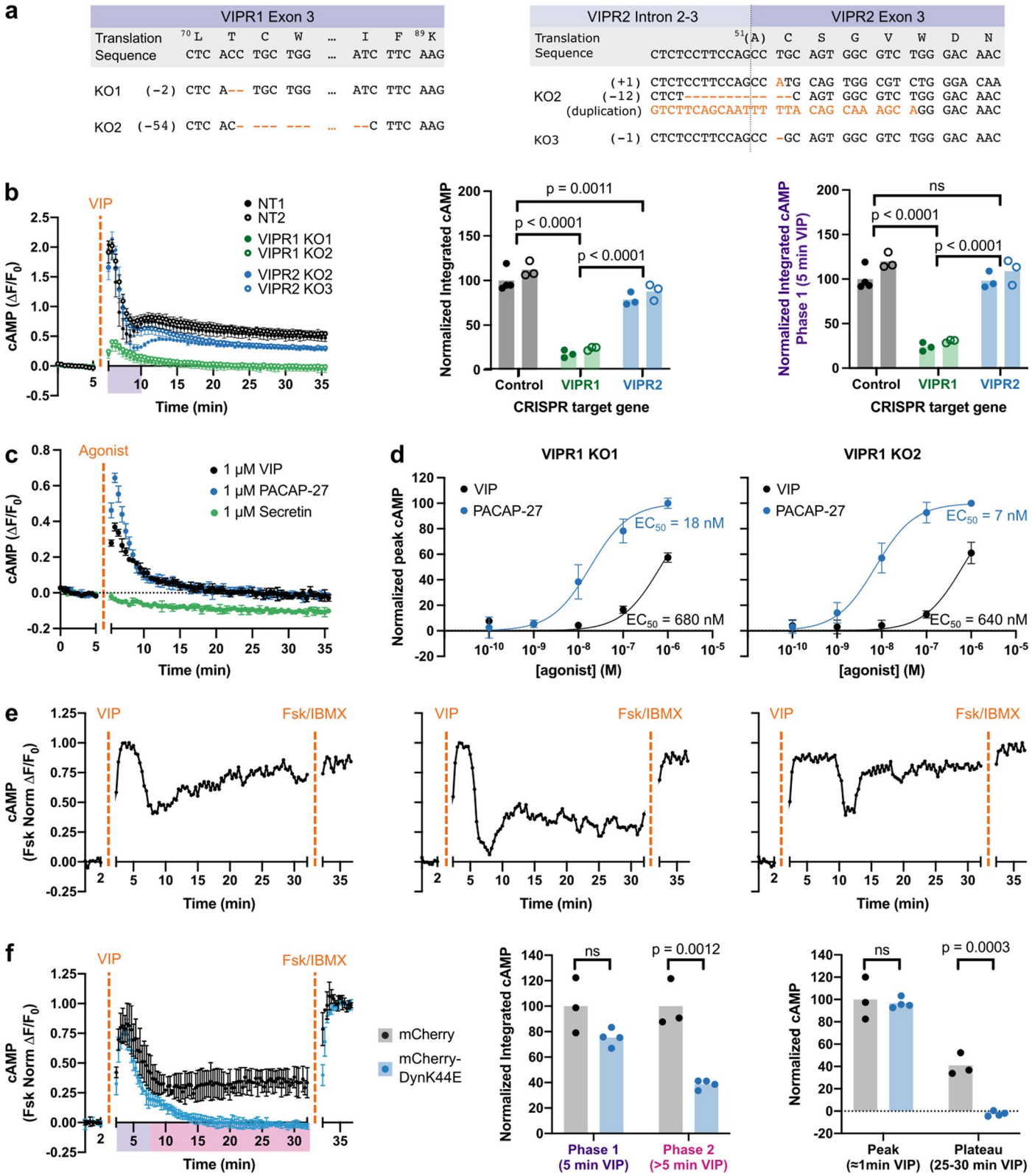

Extended Data Fig. 4 | See next page for caption.

https://doi.org/10.1038/s41589-023-01412-4

Extended Data Fig. 4 | VIPR1 mediates both phases of cAMP signaling. **a**, Alignments showing the genetic modifications of VIPR1 and VIPR2 in independent monoclonal lines. **b**, Changes in cAMP in control (NT, black), VIPR1 KO (green), and VIPR2 KO (blue) cell lines upon treatment with 500 nM VIP added at 5 minutes. Integrated cAMP of the entire timecourse and 0–5 min VIP treatment were calculated as the area under the curve and normalized to the average of NT1. Significance was determined by two-way ANOVAs with Tukey's multiple comparisons tests. Closed and open circles refer to two independent clonal cell lines. **c**, Change in cAMP in VIPR1 KO1 cell line when stimulated with 1 μM VIP (black), PACAP (blue), or secretin (green). **d**, Dose response curves for stimulation of VIPR1 KO1 and KO2 cell lines with VIP (black) or PACAP (blue). Peak cAMP, normalized to the average maximum response elicited by 1 μM PACAP, is plotted. EC_{50} were calculated as noted in Methods. **e**, Example changes in cAMP in individual cells co-expressing mCherry upon treatment with 1 μM VIP added at 2 minutes and forskolin (Fsk, 10 μM) and IBMX (500 μM) at 32 minutes. Fluorescence was measured by microscopy and normalized to maximum fluorescence change of the ROI. Corresponding aggregate data is shown in **f**. **f**, Changes in cAMP in cells expressing mCherry-Dyn1K44E (blue, n = 4) or mCherry (black, n = 3) upon treatment with 1 μM VIP added at 2 minutes. Fluorescence was measured by microscopy and normalized to fluorescence change upon co-application of forskolin (Fsk, 10 μM) and IBMX (500 μM) at 32 minutes. Integrated cAMP and peak/plateau $\Delta F/F_0$ were quantified as in Fig. 2a, with data normalized to the mCherry average. Significance was determined by unpaired two-sided t-tests. For (**b**–**d**), data represent three biological replicates shown as individual data points or mean ± s.d.

https://doi.org/10.1038/s41589-023-01412-4

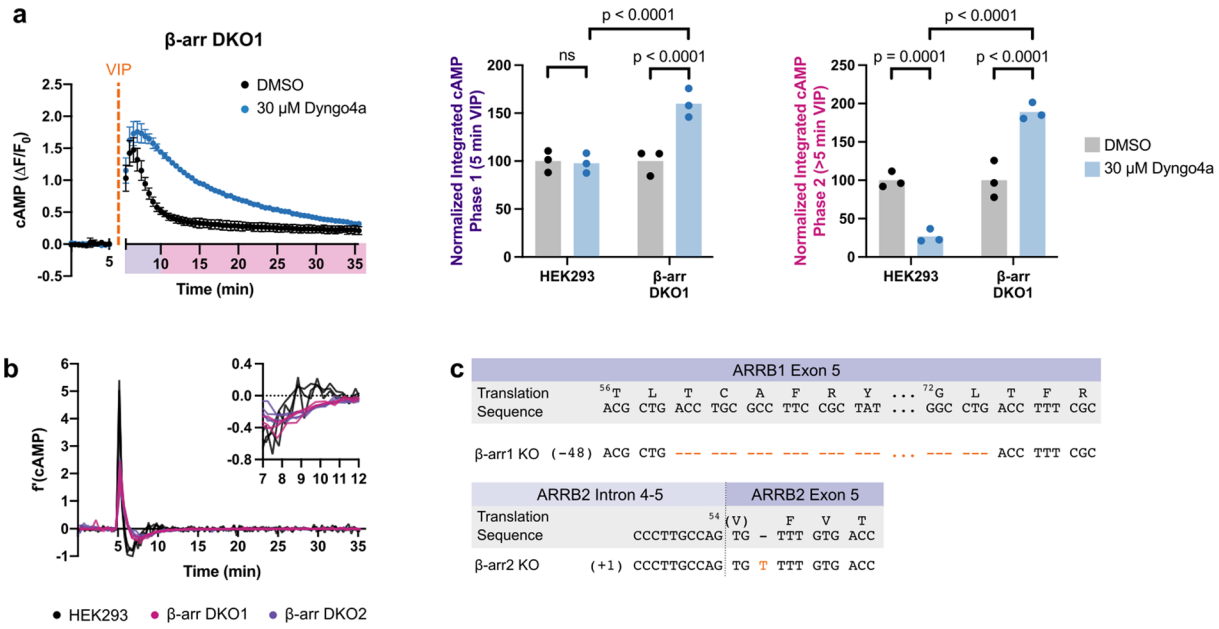

Extended Data Fig. 5 | Independent β-arr1/2 DKO cell line recapitulates cAMP signaling trends. a, Changes in cAMP in β-arr DKO1 cells upon treatment with 500 nM VIP added at 5 minutes. Integrated cAMP of each phase was calculated as the area under the curve and normalized to the average DMSO value for each cell line. Data for WT HEK293 repeated from Fig. 2a. Significance was determined by two-way ANOVA with Tukey's multiple comparisons test along with data shown in Fig. 3b. n = 3. **b**, First derivatives of each cAMP replicate time course measured in HEK293 (black), β-arr DKO1 (pink), and β-arr DKO2 (purple) cells, with timepoints between 7–12 minutes highlighted in the right panel. Data from (**a**), Fig. 2a, and Fig. 3a. **c**, Alignments showing the genetic modifications of β-arr1 (ARRB1) and β-arr2 (ARRB2) in monoclonal knockout lines. **d**, Western blot of parental HEK293 and β-arr1/2 KO cell lysates, probing for β-arrestin1/2 and α-tubulin as a loading control. Quantification of blots from three independent samples, normalizing to loading and the HEK293 parental cell line, is shown on right. **e-f**, NanoBiT bystander assays showing endosomal recruitment of mini-G_s (**e**, n = 4) or Nb37 (**f**, n = 3) upon addition of 1 μM VIP at 5 minutes in β-arr DKO1 cells. For all panels, data represent biological replicates and are shown as individual data points or mean ± s.d.

https://doi.org/10.1038/s41589-023-01412-4

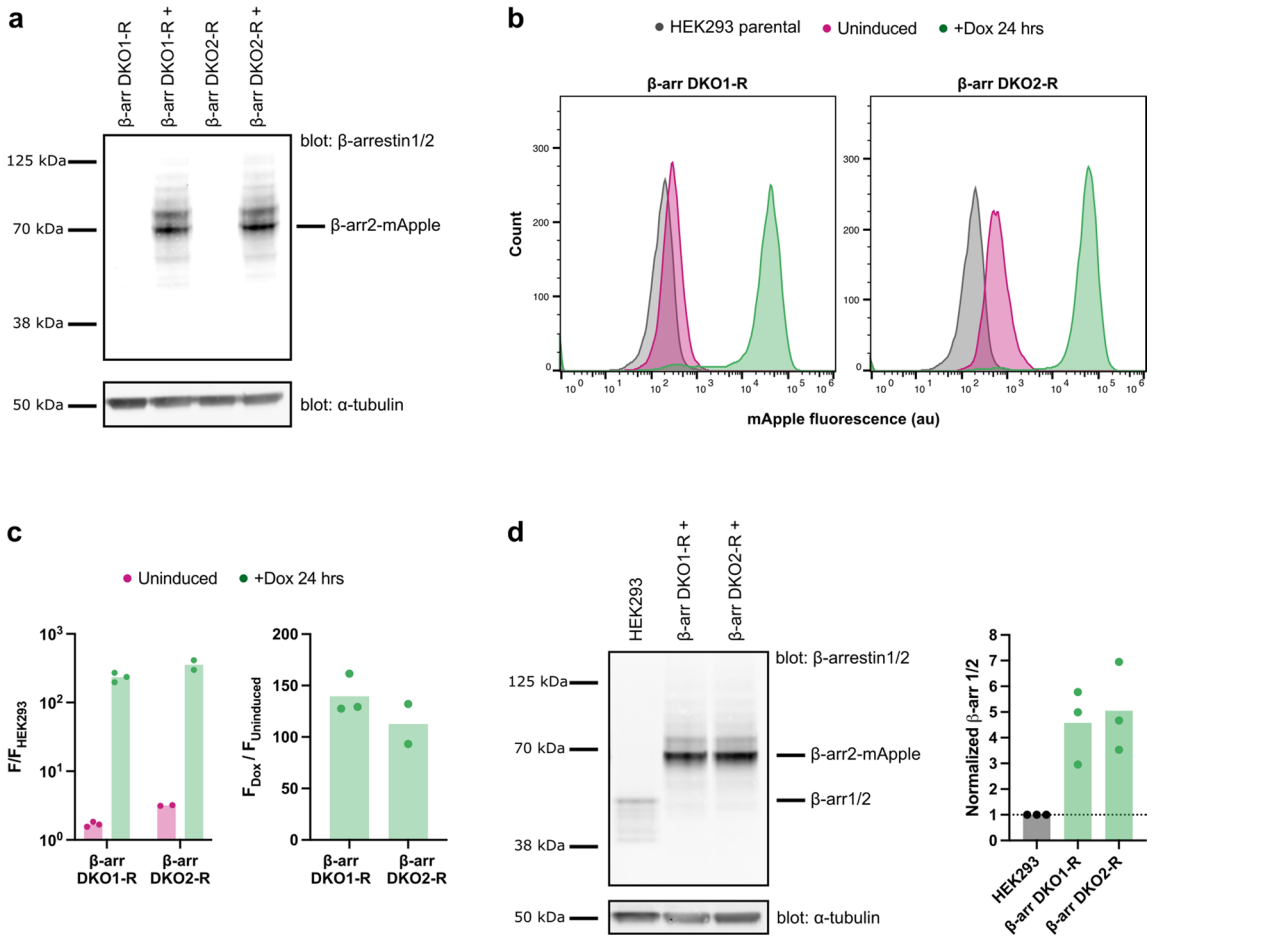

Extended Data Fig. 6 | Characterization of β-arr1/2 DKO rescue cell lines. **a**, Western blot of β-arr1/2 DKO-R cell lysates, probing for β-arr1/2 and α-tubulin as a loading control. Rescue cell lines stably express β-arr2-mApple under the control of a tet-inducible promoter (P_{TRE3GS}). For induction ('+'), cells were treated with doxycycline (Dox) for 24 hours. Blot is representative of three independent experiments. **b**, Representative flow cytometry data showing the expression of β-arr2 upon dox induction, as measured by mApple fluorescence. **c**, Quantification of flow cytometry data shown in (**b**). Ratios of the median mApple fluorescence are shown compared to parental HEK293 cells (right) and the uninduced β-arr1/2 DKO-R cell lines (left). **d**, Western blot of parental HEK293 cells and induced β-arr1/2 DKO-R cells, probing for β-arr1/2 and α-tubulin as a loading control. Quantification of blots from three independent inductions, normalizing to loading and the HEK293 parental cell line, is shown on right. For all panels, data represent biological replicates and are shown as individual data points.

https://doi.org/10.1038/s41589-023-01412-4

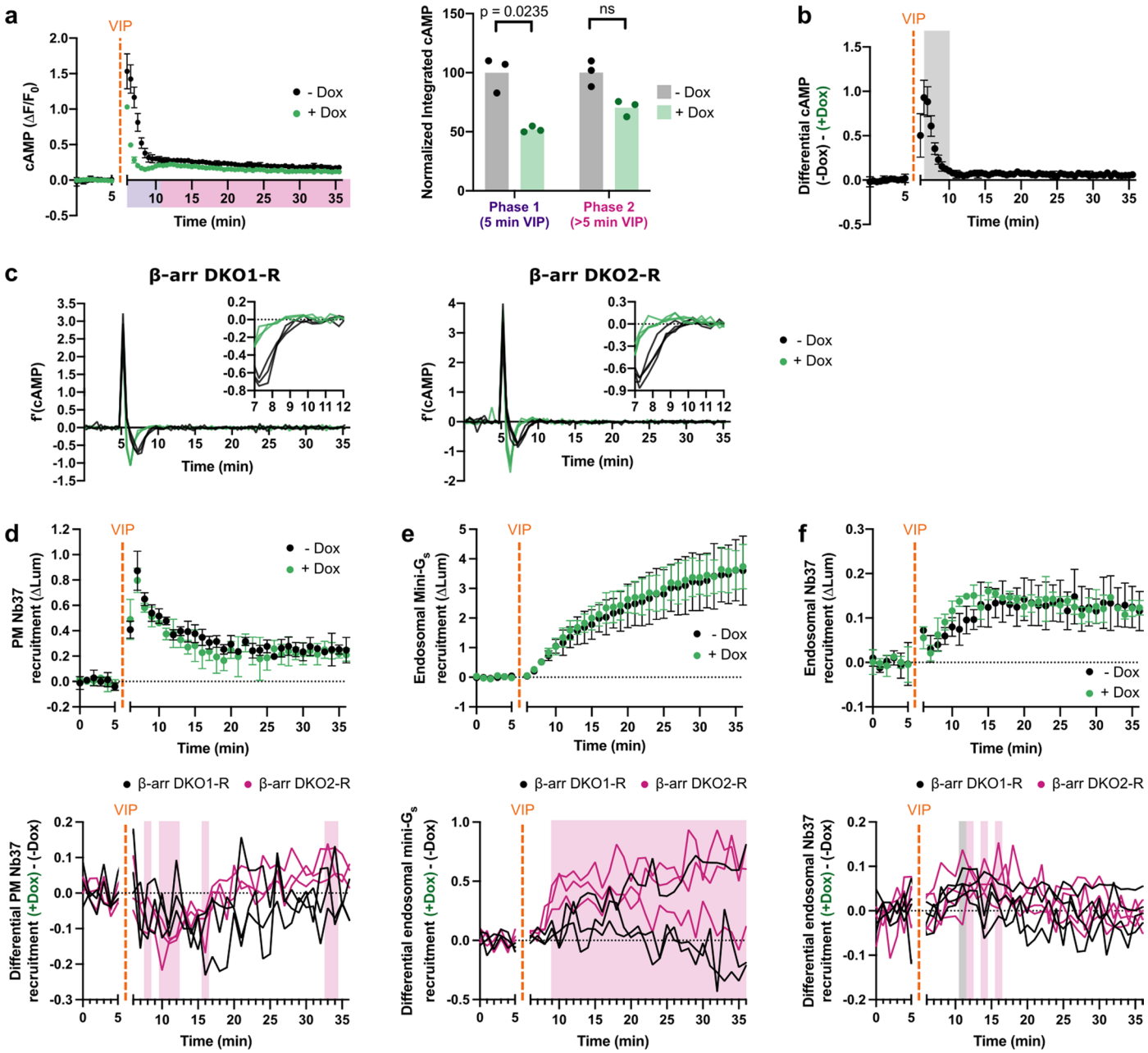

Extended Data Fig. 7 | Two independent β-arr1/2 DKO-R cell lines demonstrate β-arrestin's role in desensitizing the first phase of VIPR1 signaling. a, Changes in cAMP in β-arr DKO1-R cells with (green) and without (black) Dox induction upon treatment with 500 nM VIP added at 5 minutes. Integrated cAMP of each phase (0–5 min or 5–30 min VIP treatment) was calculated as the area under the curve and normalized to the average -Dox value. Significance was determined by a repeated measures 2 way ANOVA with Sidak's multiple comparisons test along with data for DKO2-R shown in Fig. 4a. n = 3. **b**, Difference in cAMP response with and without β-arr2 expression, calculated as the difference in fluorescence change ($\Delta F/F_0$) between the -Dox and +Dox curves shown in (**a**). Shaded area represents timepoints where the difference is statistically significant, as determined by a repeated measures 2 way ANOVA with Sidak's multiple comparisons test ($p < 0.05$) carried out on the curves in (**a**). n = 3. **c**, First derivatives of each cAMP replicate time course measured in β-arr DKO2-R (Fig. 4a) and β-arr DKO1-R (**a**). **d**–**f**, NanoBiT bystander assays showing plasma membrane recruitment of Nb37 (**d**, n = 3) or endosomal recruitment of mini-G_s (**e**, n = 3) and SmBiT (**f**, n = 4) in β-arr DKO1-R cells upon addition of 1 μM VIP at 5 minutes. Shown below each panel is the differential recruitment, calculated as the difference between +Dox and -Dox curves, for both β-arr DKO1-R (black) and β-arr DKO2-R (pink, Fig. 4c–e) cell lines. Shaded areas represent timepoints where the difference is statistically significant, as determined by a repeated measures 2 way ANOVA with Sidak's multiple comparisons test ($p < 0.05$), for β-arr DKO1-R (black) and β-arr DKO2-R (pink). For all panels, cells treated with Dox to induce expression of β-arr2-mApple are shown in green, and data represent biological replicates, shown as individual data points or mean ± s.d.

https://doi.org/10.1038/s41589-023-01412-4

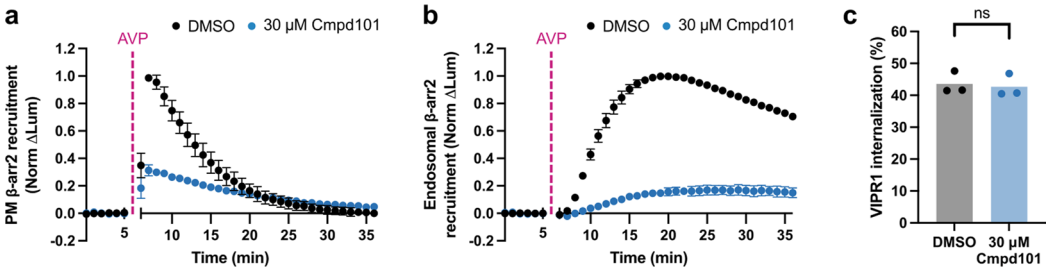

Extended Data Fig. 8 | Cmpd101 differentially modulates receptor-β-arrestin complexes. a, **b**, NanoBiT bystander assays showing plasma membrane (**a**) or endosomal (**b**) recruitment of β-arr2 in HEK293 cells overexpressing V2R upon addition of 1 μM AVP at 5 minutes. **c**, Internalization of HaloTag-VIPR1 after a 30 minute treatment with 500 nM VIP, as measured by flow cytometry. Significance was determined by a paired two-sided t-test. For all panels, data represent three biological replicates shown as individual data points or mean ± s.d.

nature portfolio

Corresponding author(s): Mark von Zastrow

Last updated by author(s): 07/05/2023

Reporting Summary

Nature Portfolio wishes to improve the reproducibility of the work that we publish. This form provides structure for consistency and transparency in reporting. For further information on Nature Portfolio policies, see our Editorial Policies and the Editorial Policy Checklist.

Statistics

For all statistical analyses, confirm that the following items are present in the figure legend, table legend, main text, or Methods section.

n/a	Confirmed
☐	☒ The exact sample size (*n*) for each experimental group/condition, given as a discrete number and unit of measurement
☐	☒ A statement on whether measurements were taken from distinct samples or whether the same sample was measured repeatedly
☐	☒ The statistical test(s) used AND whether they are one- or two-sided *Only common tests should be described solely by name; describe more complex techniques in the Methods section.*
☐	☒ A description of all covariates tested
☐	☒ A description of any assumptions or corrections, such as tests of normality and adjustment for multiple comparisons
☐	☒ A full description of the statistical parameters including central tendency (e.g. means) or other basic estimates (e.g. regression coefficient) AND variation (e.g. standard deviation) or associated estimates of uncertainty (e.g. confidence intervals)
☐	☒ For null hypothesis testing, the test statistic (e.g. *F*, *t*, *r*) with confidence intervals, effect sizes, degrees of freedom and *P* value noted *Give P values as exact values whenever suitable.*
☒	☐ For Bayesian analysis, information on the choice of priors and Markov chain Monte Carlo settings
☒	☐ For hierarchical and complex designs, identification of the appropriate level for tests and full reporting of outcomes
☐	☒ Estimates of effect sizes (e.g. Cohen's *d*, Pearson's *r*), indicating how they were calculated

Our web collection on statistics for biologists contains articles on many of the points above.

Software and code

Policy information about availability of computer code

Data collection	NIS Elements HC v5.21.03 (Nikon), Micromanager v1.4.23, Gen5 v2.05 (BioTek), Attune Cytometric Software v5.3.2415.0 (Thermo Fisher), Odyssey v2.0.3 (LI-COR Biosciences)
Data analysis	Cell Profiler 4, Fiji v1.53, FlowJo v10.8 (BD Life Sciences), Prism v8 and v9 (GraphPad), Synthego ICE Analysis Tool

For manuscripts utilizing custom algorithms or software that are central to the research but not yet described in published literature, software must be made available to editors and reviewers. We strongly encourage code deposition in a community repository (e.g. GitHub). See the Nature Portfolio guidelines for submitting code & software for further information.

Data

Policy information about availability of data

All manuscripts must include a data availability statement. This statement should provide the following information, where applicable:

- Accession codes, unique identifiers, or web links for publicly available datasets
- A description of any restrictions on data availability
- For clinical datasets or third party data, please ensure that the statement adheres to our policy

Data and uncropped blots for Figs. 1–5 and Extended Data Figs. 1–2,4-8 are provided with this paper as source data files.

Human research participants

Policy information about studies involving human research participants and Sex and Gender in Research.

Reporting on sex and gender	Not applicable.
Population characteristics	Not applicable.
Recruitment	Not applicable.
Ethics oversight	Not applicable.

Note that full information on the approval of the study protocol must also be provided in the manuscript.

Field-specific reporting

Please select the one below that is the best fit for your research. If you are not sure, read the appropriate sections before making your selection.

☒ Life sciences ☐ Behavioural & social sciences ☐ Ecological, evolutionary & environmental sciences

For a reference copy of the document with all sections, see nature.com/documents/nr-reporting-summary-flat.pdf

Life sciences study design

All studies must disclose on these points even when the disclosure is negative.

Sample size	Sample sizes were chosen according to the current standards of the field and verified by experience in our lab in the present experimental system (ex. PMID 33649598). For all experiments, at least three independent biological replicates, defined as samples from separate preparations on different days, were analyzed. Each biological replicate represents the mean of at least two technical replicates, defined as samples from the same preparation analyzed on the same day.
Data exclusions	No data were excluded from analysis.
Replication	All experiments were carried out at least three times, and all findings in the manuscript were reproducible.
Randomization	This is not relevant to the study because all experiments were done in the same cell line background.
Blinding	Blinding was not done during data collection or analysis. Blinding is not relevant as most of the data collection and analysis methods are not vulnerable to human bias. The only results potentially subject to human bias are the microscopy-based colocalization experiments. Accordingly, all colocalization experiments were verified using an orthogonal method (NanoBiT) that is inherently unbiased.

Reporting for specific materials, systems and methods

We require information from authors about some types of materials, experimental systems and methods used in many studies. Here, indicate whether each material, system or method listed is relevant to your study. If you are not sure if a list item applies to your research, read the appropriate section before selecting a response.

Materials & experimental systems

n/a	Involved in the study
☐	☒ Antibodies
☐	☒ Eukaryotic cell lines
☒	☐ Palaeontology and archaeology
☒	☐ Animals and other organisms
☒	☐ Clinical data
☒	☐ Dual use research of concern

Methods

n/a	Involved in the study
☒	☐ ChIP-seq
☐	☒ Flow cytometry
☒	☐ MRI-based neuroimaging

Antibodies

Antibodies used	anti-b-arrestin1/2 (Cell Signaling Technologies cat# 4674, clone D24H9) anti-tubulin (Cell Signaling Technologies cat# 3873, clone DM1A) IRDye 680RD Donkey anti-Mouse IgG (LI-COR Biosciences cat# 926-68072)

IRDye 800CW Donkey anti-Rabbit IgG (LI-COR Biosciences cat# 926-32213)
anti-FLAG (Sigma Aldrich cat# F3040, clone M1)
anti-LgBiT (Promega cat# N7100)
anti-EEA1 (Santa Cruz Biotechnology cat# sc-6415)
Donkey anti goat IgG AlexaFluor 488 (Invitrogen cat# A-11055)
Donkey anti mouse IgG AlexaFluor 647 (Invitrogen cat# A-31571)

Validation

All antibodies are commercially available and have been previously validated/published, according to manufacturer's websites:
anti-b-arrestin1/2: https://www.cellsignal.com/products/primary-antibodies/b-arrestin-1-2-d24h9-rabbit-mab/4674
anti-tubulin: https://www.cellsignal.com/products/primary-antibodies/a-tubulin-dm1a-mouse-mab/3873
IRDye 680RD Donkey anti-Mouse IgG: https://www.licor.com/bio/reagents/irdye-680rd-donkey-anti-mouse-igg-secondary-antibody
IRDye 800CW Donkey anti-Rabbit IgG: https://www.licor.com/bio/reagents/irdye-800cw-donkey-anti-rabbit-igg-secondary-antibody
anti-FLAG: https://www.sigmaaldrich.com/US/en/product/sigma/f3040
anti-LgBiT: https://www.promega.com/products/protein-detection/primary-and-secondary-antibodies/anti-lgbit-monoclonal-antibody/?catNum=N7100
anti-EEA1: https://www.scbt.com/p/eea1-antibody-n-19
Donkey anti goat IgG AlexaFluor 488: https://www.thermofisher.com/antibody/product/Donkey-anti-Goat-IgG-H-L-Cross-Adsorbed-Secondary-Antibody-Polyclonal/A-11055
Donkey anti mouse IgG AlexaFluor 647: https://www.thermofisher.com/antibody/product/Donkey-anti-Mouse-IgG-H-L-Highly-Cross-Adsorbed-Secondary-Antibody-Polyclonal/A-31571

Eukaryotic cell lines

Policy information about cell lines and Sex and Gender in Research

Cell line source(s)	All cell lines, including VIPR1 and β-arrestin knockout cell lines, were derived from HEK293 cell line from ATCC (CRL-1573), except for GRK2/3/5/6 KO cell line which is from A. Inoue (Kawakami, K. et al. Heterotrimeric Gq proteins act as a switch for GRK5/6 selectivity underlying β-arrestin transducer bias. Nat. Commun. 13, 487 (2022)).
Authentication	Not authenticated.
Mycoplasma contamination	All cell lines tested negative for mycoplasma.
Commonly misidentified lines (See ICLAC register)	No commonly misidentified lines were used.

Flow Cytometry

Plots

Confirm that:

☒ The axis labels state the marker and fluorochrome used (e.g. CD4-FITC).

☒ The axis scales are clearly visible. Include numbers along axes only for bottom left plot of group (a 'group' is an analysis of identical markers).

☒ All plots are contour plots with outliers or pseudocolor plots.

☒ A numerical value for number of cells or percentage (with statistics) is provided.

Methodology

Sample preparation	HEK293 cultured cells were enzymatically lifted. When appropriate, cells were labeled with HaloTag ligands.
Instrument	Attune NxT (Thermo Fisher)
Software	Attune NxT Software (Thermo Fisher)
Cell population abundance	HEK293 cultured cells stably overexpressing GPCRs of interest were used, and as such, no gating was needed to select for receptor-positive cells. When cells were also overexpressing mCherry or mCherry-Dyn1K44E via BacMam, cells were gated for mCherry expression.
Gating strategy	FSC-A vs. SSC-A and FSC-A vs. FSC-H gates were used to identify single cell populations. In the case where mCherry(Dyn1K44E) was also expressed, an mCherry+ gate was used to select for cells with similar levels of mCherry fluorescence.

☒ Tick this box to confirm that a figure exemplifying the gating strategy is provided in the Supplementary Information.